

One-loop corrections to the Higgs boson invisible decay in a complex singlet extension of the SM

Felix Egle,^{1,*} Margarete Mühlleitner,^{1,†} Rui Santos^{2,3,‡} and João Viana^{2,§}

¹*Institute for Theoretical Physics, Karlsruhe Institute of Technology,
Wolfgang-Gaede-Strasse 1, 76131 Karlsruhe, Germany*

²*Centro de Física Teórica e Computacional, Faculdade de Ciências, Universidade de Lisboa,
Campo Grande, Edifício C8, 1749-016 Lisboa, Portugal*

³*ISEL - Instituto Superior de Engenharia de Lisboa, Instituto Politécnico de Lisboa,
1959-007 Lisboa, Portugal*



(Received 12 February 2022; accepted 1 November 2022; published 28 November 2022)

The search for dark matter (DM) at colliders is founded on the idea of looking for something invisible. There are searches based on production and decay processes where DM may reveal itself as missing energy. If nothing is found, our best tool to constrain the parameter space of many extensions of the Standard Model (SM) with a DM candidate is the Higgs boson. As the measurements of the Higgs couplings become increasingly precise, higher-order corrections will start to play a major role. The tree-level contribution to the invisible decay width provides information about the portal coupling. Higher-order corrections also give us access to other parameters from the dark sector of the Higgs potential that are not present in the tree-level amplitude. In this work we will focus on the complex singlet extension of the SM in the phase with a DM candidate. We calculate the one-loop electroweak corrections to the decay of the Higgs boson into two DM particles. We find that the corrections are stable and of the order of a few percent. The present measurement of the Higgs invisible branching ratio, $\text{BR}(H \rightarrow \text{invisible}) < 0.11$, already constrains the parameter space of the model at leading order. We expect that by the end of the LHC the experimental measurement will require the inclusion of the electroweak corrections to the decay in order to match the experimental accuracy. Furthermore, the only competing process, which is direct detection, is shown to have a cross section below the neutrino floor.

DOI: [10.1103/PhysRevD.106.095030](https://doi.org/10.1103/PhysRevD.106.095030)

I. INTRODUCTION

The determination of the scalar potential and the search for dark matter (DM) have replaced the search for the Higgs boson as the main goal of particle physicists. In fact, since the Higgs has been discovered at the Large Hadron Collider (LHC) by the ATLAS [1] and CMS [2] Collaborations, and the Higgs couplings have been measured with great precision, the attention has turned to the outstanding problems of the Standard Model (SM). The search for DM is certainly on the top of the list especially because at this point we cannot even be sure if it comes in the form of an elementary particle. Therefore, even if collider physics is

not the place to prove the existence of a DM candidate, it can help us by hinting at some particular directions even if only by excluding the parameter space of particular models. The Higgs invisible decay measurements are probably one of the best quantities to probe the dark sector of particular models. The branching ratio of Higgs to invisible is now bounded to below 11% by ATLAS [3]. This number will improve both in the next LHC run and in the high luminosity stage. This increasing precision will take us further inside the dark sector of the models.

In this work we discuss the Higgs invisible decay in the complex singlet extension of the SM (CxSM) which amounts to the addition of a complex scalar singlet to the known SM fields while keeping the SM gauge symmetries. While the tree-level decay of the Higgs into DM involves only the portal coupling, the one-loop corrections to the decay give us access to the quartic coupling of the singlet field (for a review on scalar portal models see [4,5]). Therefore, the one-loop result gives us a more complete understanding of the Higgs potential. The computation of the one-loop corrections for the Higgs decay into DM particles for the dark doublet phase of the

*felix.egle@kit.edu

†margarete.muehlleitner@kit.edu

‡rasantos@fc.ul.pt

§jfvvchico@hotmail.com

Published by the American Physical Society under the terms of the Creative Commons Attribution 4.0 International license. Further distribution of this work must maintain attribution to the author(s) and the published article's title, journal citation, and DOI. Funded by SCOAP³.

Next-to-minimal two-Higgs doublet model (N2HDM) was already performed in Ref. [6]. There is a competing and complementary measurement that is the direct detection process. The DM-nucleon cross section is only relevant at one-loop due to a cancellation that renders the tree-level cross section proportional to the DM velocity and therefore negligible [7,8]. The one-loop corrections to the direct detection process were calculated in [9,10] and compared to the latest experimental results from XENON [11]. We will discuss the interplay between direct detection and the branching ratio of the invisible Higgs decay including the electroweak corrections in both processes.

This special feature of having a negligible DM-nucleon cross section occurs only in the CxSM with a softly broken (by dimension two terms) $U(1)$ symmetry. This is the main difference when we compare this model with the real singlet extension of the SM. For a review of the DM real singlet extension see [12,13], and for a previous study of the phenomenology of the CxSM see [14].

Our analysis will be performed taking into account the most relevant theoretical and experimental constraints on the model. These are collider constraints and also DM constraints. We will then calculate the next-to-leading order (NLO) electroweak corrections to the invisible decay width of the SM-like Higgs boson using several renormalization schemes. Once the allowed parameter space is found, the NLO result will be compared with the leading order (LO) one. The final goal is to understand if the NLO Higgs branching ratio into two DM particles can be larger than the LO one and will hence be constrained by the experimentally measured value that is fulfilled by the LO one for our chosen parameter points. Moreover, as the new data will become available both at the next LHC run and at the high luminosity stage, the Higgs coupling measurements will be more precise and the theoretical calculations need to match this precision.

The outline of the paper is as follows. In Sec. II, we will introduce the CxSM together with our notation. Section III is dedicated to the description of the different renormalization schemes used in this work. Section IV discusses the experimental and theoretical constraints on the model. In Sec. V, the results are presented and discussed. Our conclusions are collected in Sec. VI. Finally, there are two appendixes. In the first one we present the results of the scalar pinched self-energies. In the second one we discuss the stability of the different minima of the CxSM potential.

II. THE CxSM POTENTIAL

In this section we introduce the version of the CxSM used in this work. The model is a simple extension of the SM where a complex singlet field with zero isospin and zero hypercharge is added to the model. As a singlet for the SM gauge group, the scalar field appears only in the Higgs potential. The SM Higgs couplings will, however, be modified by the rotation angle from the matrix that relates

the scalar gauge eigenstates with their mass eigenstates. The doublet field Φ and the singlet field \mathbb{S} are defined as

$$\begin{aligned}\Phi &= \begin{pmatrix} G^+ \\ \frac{1}{\sqrt{2}}(v + H + iG^0) \end{pmatrix}, \\ \mathbb{S} &= \frac{1}{\sqrt{2}}(v_S + S + i(v_A + A)),\end{aligned}\quad (1)$$

where H , S , and A are real scalar fields and G^+ and G^0 are the Goldstone bosons for the Z and W^\pm bosons. The v , v_A , and v_S are the vacuum expectation values (VEVs) of the corresponding fields and can all be, in general, nonzero in which case mixing between all three scalar fields arises. We will, however, focus on a model where a DM candidate is generated by forcing the potential to be invariant under a symmetry, unbroken by the vacuum. We choose to impose invariance of the potential under two separate \mathbb{Z}_2 symmetries acting on S and A , that is, $S \rightarrow -S$ and $A \rightarrow -A$. The resulting renormalizable potential is

$$\begin{aligned}V &= \frac{m^2}{2} \Phi^\dagger \Phi + \frac{\lambda}{4} (\Phi^\dagger \Phi)^2 + \frac{\delta_2}{2} \Phi^\dagger \Phi |\mathbb{S}|^2 + \frac{b_2}{2} |\mathbb{S}|^2 \\ &\quad + \frac{d_2}{4} |\mathbb{S}|^4 + \left(\frac{b_1}{4} \mathbb{S}^2 + \text{c.c.} \right),\end{aligned}\quad (2)$$

where all constants are real. By choosing $v_A = 0$, the $A \rightarrow -A$ symmetry remains unbroken and A is stable, becoming the DM candidate of the model. The other \mathbb{Z}_2 symmetry is broken since $v_S \neq 0$, which leads to mixing between S and H . The mass eigenstates of the CP -even field h_i ($i = 1, 2$) relate to the gauge eigenstates H and S through

$$\begin{pmatrix} h_1 \\ h_2 \end{pmatrix} = R_\alpha \begin{pmatrix} H \\ S \end{pmatrix},\quad (3)$$

where the rotation matrix is given by

$$R_\alpha = \begin{pmatrix} \cos \alpha & \sin \alpha \\ -\sin \alpha & \cos \alpha \end{pmatrix} \equiv \begin{pmatrix} c_\alpha & s_\alpha \\ -s_\alpha & c_\alpha \end{pmatrix}.\quad (4)$$

The mass matrix in the gauge basis (H, S) is given by

$$\mathcal{M} = \begin{pmatrix} \frac{v^2 \lambda}{2} & \frac{\delta_2 v v_S}{2} \\ \frac{\delta_2 v v_S}{2} & \frac{d_2 v_S^2}{2} \end{pmatrix} + \begin{pmatrix} \frac{T_1}{v} & 0 \\ 0 & \frac{T_2}{v_S} \end{pmatrix},\quad (5)$$

where the tadpole parameters T_1 and T_2 are defined via the minimization conditions,

$$\frac{\partial V}{\partial v} \equiv T_1 \Rightarrow \frac{T_1}{v} = \frac{m^2}{2} + \frac{\delta_2 v_S^2}{4} + \frac{v^2 \lambda}{4},\quad (6a)$$

$$\frac{\partial V}{\partial v_S} \equiv T_2 \Rightarrow \frac{T_2}{v_S} = \frac{b_1 + b_2}{2} + \frac{\delta_2 v^2}{4} + \frac{v_S^2 d_2}{4},\quad (6b)$$

and at tree level, the minimum conditions are $T_i = 0$ ($i = 1, 2$). The mass of the DM candidate A is given by

$$m_A^2 = \frac{-b_1 + b_2}{2} + \frac{\delta_2 v^2}{4} + \frac{v_S^2 d_2}{4} = -b_1 + \frac{T_2}{v_S}, \quad (7)$$

while the remaining mass eigenstates are obtained via

$$D_{hh}^2 \equiv R_\alpha \mathcal{M} R_\alpha^T, \quad D_{hh}^2 = \text{diag}(m_{h_1}^2, m_{h_2}^2). \quad (8)$$

Therefore, the scalar spectrum of the CxSM consists of two Higgs bosons, h_1 and h_2 , one of which is the SM-like Higgs with a mass of 125 GeV, and one DM scalar, which we call A . Since the mixing between the two scalars is introduced only via the rotation angle, the couplings of the two Higgs bosons to the remaining SM particles is modified by the same factor k_i defined as

$$g_{h_i \text{SMSM}} = g_{H_{\text{SM}} \text{SMSM}} k_i, \quad k_i \equiv \begin{cases} \cos \alpha, & i = 1 \\ -\sin \alpha, & i = 2 \end{cases}, \quad (9)$$

where $g_{H_{\text{SM}} \text{SMSM}}$ denotes the SM coupling between the SM Higgs and the SM particle SM .

With these definitions the parameters of the potential can now be written as functions of our choice of input parameters given by

$$v, \quad v_S, \quad \alpha, \quad m_{h_1}, \quad m_{h_2}, \quad m_A, \quad (10)$$

as

$$\lambda = \frac{m_{h_1}^2 + m_{h_2}^2 + \cos 2\alpha(m_{h_1}^2 - m_{h_2}^2)}{v^2}, \quad (11a)$$

$$d_2 = \frac{m_{h_1}^2 + m_{h_2}^2 + \cos 2\alpha(m_{h_2}^2 - m_{h_1}^2)}{v_S^2}, \quad (11b)$$

$$\delta_2 = \frac{(m_{h_1}^2 - m_{h_2}^2) \sin 2\alpha}{v v_S}, \quad (11c)$$

$$m^2 = \frac{1}{2} \left(\cos 2\alpha(m_{h_2}^2 - m_{h_1}^2) - \frac{v(m_{h_1}^2 + m_{h_2}^2) + v_S(m_{h_1}^2 - m_{h_2}^2) \sin 2\alpha}{v} \right), \quad (11d)$$

$$b_2 = \frac{1}{2} \left(2m_A^2 - m_{h_1}^2 - m_{h_2}^2 + \cos 2\alpha(m_{h_1}^2 - m_{h_2}^2) - \frac{v(m_{h_1}^2 - m_{h_2}^2) \sin 2\alpha}{v_S} \right), \quad (11e)$$

$$b_1 = -m_A^2. \quad (11f)$$

Note that the model depends only on four independent parameters, because one of the Higgs bosons plays the role of the SM-like Higgs with a mass of 125 GeV and the doublet VEV $v = 1/\sqrt{\sqrt{2}G_F} \approx 246.22$ GeV, where G_F denotes the Fermi constant. The VEV is replaced by G_F as an input parameter.

III. RENORMALIZATION

Our goal is to calculate the decay width of the Higgs bosons into a pair of DM particles, $h_i \rightarrow AA$, at NLO. Since A only couples to the two Higgs bosons h_i , we just need to renormalize the scalar sector. With the trilinear h_i couplings to the DM particles given by

$$\lambda_{h_i AA} = \frac{m_{h_i}^2}{v_S} \begin{cases} s_\alpha, & i = 1 \\ c_\alpha, & i = 2 \end{cases}, \quad (12)$$

and according to our choice of input parameters, we need to renormalize the masses of the two scalars h_i , the mass of the DM particle m_A , the singlet VEV v_S , and the mixing angle α . Besides these parameters we also need to renormalize the h_i and A fields and the tadpoles to work with finite Green functions. We start by formally defining the relation between the bare and the renormalized quantities as

$$\beta_0 = \beta + \delta\beta, \quad (13)$$

where $\delta\beta$ is the counterterm of the physical quantity β and β_0 is the bare quantity. All bare fields ϕ_0 are related to their renormalized version via

$$\phi_0 = \sqrt{Z_\phi} \phi \approx \left(1 + \frac{\delta Z_\phi}{2} \right) \phi, \quad (14)$$

where Z_ϕ is the field strength renormalization constant.

A. On-shell renormalization of the scalar sector

We start by calculating the mass and field counterterms in the scalar sector using the on-shell scheme. The renormalization constants for the DM particle are defined as

$$A_0 = \sqrt{Z_A} A \approx \left(1 + \frac{\delta Z_A}{2} \right) A, \quad D_{A,0}^2 = D_A^2 + \delta D_A^2, \quad (15)$$

where Z_A is the field strength renormalization constant, $D_{A,0}^2 = m_{A,0}^2$, and δD_A is the mass counterterm for A .

The two scalars h_1 and h_2 again mix at one-loop order, and therefore both the field renormalization constants and the mass counterterms are defined by

$$\begin{aligned} \begin{pmatrix} h_{1,0} \\ h_{2,0} \end{pmatrix} &= \sqrt{Z_{hh}} \begin{pmatrix} h_1 \\ h_2 \end{pmatrix} \approx \left(1 + \frac{\delta Z_{hh}}{2}\right) \begin{pmatrix} h_1 \\ h_2 \end{pmatrix}, \\ D_{hh,0}^2 &= D_{hh}^2 + \delta D_{hh}^2, \end{aligned} \quad (16)$$

with $D_{hh,0}^2 = \text{diag}(m_{h_{1,0}}^2, m_{h_{2,0}}^2)$ and the matrices δZ_{hh} and δD_{hh}^2 defined as

$$\begin{aligned} \delta Z_{hh} &= \begin{pmatrix} \delta Z_{h_1 h_1} & \delta Z_{h_1 h_2} \\ \delta Z_{h_2 h_1} & \delta Z_{h_2 h_2} \end{pmatrix}, \\ \delta D_{hh}^2 &= \begin{pmatrix} \delta D_{h_1 h_1}^2 & \delta D_{h_1 h_2}^2 \\ \delta D_{h_2 h_1}^2 & \delta D_{h_2 h_2}^2 \end{pmatrix}. \end{aligned} \quad (17)$$

The on-shell renormalization conditions lead to the following expressions:

$$\delta D_{h_i h_i}^2 = \text{Re}(\Sigma_{h_i h_i}(m_{h_i}^2)), \quad (18a)$$

$$\delta Z_{h_i h_i} = -\text{Re}\left(\left.\frac{\partial \Sigma_{h_i h_i}(p^2)}{\partial p^2}\right|_{p^2=m_{h_i}^2}\right), \quad (18b)$$

$$\delta Z_{h_i h_j} = \frac{2}{m_{h_i}^2 - m_{h_j}^2} \text{Re}(\Sigma_{h_i h_j}(m_{h_j}^2) - \delta D_{h_i h_j}^2) (i \neq j), \quad (18c)$$

for the counterterms of the scalar fields h_i where $\Sigma_{h_i h_i}$ denotes their self-energies. Similarly, the expressions for the DM field A read

$$\delta D_A^2 = \text{Re}(\Sigma_A(m_A^2)), \quad (19a)$$

$$\delta Z_A = -\text{Re}\left(\left.\frac{\partial \Sigma_A(p^2)}{\partial p^2}\right|_{p^2=m_A^2}\right). \quad (19b)$$

The diagonal terms of δD_{hh}^2 or δD_A^2 are related to the mass counterterms and to the corresponding tadpoles. The off-diagonal terms are related to the tadpoles to be discussed in the next section.

B. Tadpole renormalization

Tadpole renormalization is essentially the way we choose the VEVs at one-loop order so that the minimum conditions hold. Another way to express it is to state that the terms proportional to the scalar fields at one-loop order have to vanish. The VEV chosen to fulfill this condition [15,16] is the true VEV of the theory. We will follow the scheme proposed by Fleischer and Jegerlehner [15] for the SM with the goal of rendering all counterterms related to physical quantities gauge independent. The scheme was applied to various extensions of the SM (see, e.g., [17,18]). For the CxSM a brief description follows. We start by defining the true VEVs by performing the shifts

$$v \rightarrow v + \Delta v, \quad (20a)$$

$$v_S \rightarrow v_S + \Delta v_S, \quad (20b)$$

which lead to the following shifts in the tadpole parameters at NLO:

$$T_1 \rightarrow T_1 + \frac{v^2 \lambda}{2} \Delta v + \frac{\delta_2 v v_S}{2} \Delta v_S \equiv T_1 + \delta T_1, \quad (21a)$$

$$T_2 \rightarrow T_2 + \frac{\delta_2 v v_S}{2} \Delta v + \frac{d_2 v_S^2}{2} \Delta v_S \equiv T_2 + \delta T_2. \quad (21b)$$

The minimum equations lead to the following relations between the shifts in the VEVs and the tadpole counterterms:

$$\begin{pmatrix} \Delta v \\ \Delta v_S \end{pmatrix} = R_\alpha^T \begin{pmatrix} \frac{\delta T_{h_1}}{m_{h_1}^2} \\ \frac{\delta T_{h_2}}{m_{h_2}^2} \end{pmatrix}, \quad (22)$$

with the relation between the tadpole counterterms $\delta T_{1,2}$ in the gauge basis and those in the mass basis, $\delta T_{h_{1,2}}$, given by

$$\begin{pmatrix} \delta T_1 \\ \delta T_2 \end{pmatrix} = R_\alpha^T \begin{pmatrix} \delta T_{h_1} \\ \delta T_{h_2} \end{pmatrix}. \quad (23)$$

The shift introduced in the VEVs can be applied to the mass matrix from Eq. (5). The additional terms resulting from that shift read

$$\begin{aligned} \mathcal{M} \rightarrow \mathcal{M} + \begin{pmatrix} v \Delta v \lambda & \frac{\delta_2}{2} (\Delta v v_S + v \Delta v_S) \\ \frac{\delta_2}{2} (\Delta v v_S + v \Delta v_S) & d_2 v_S \Delta v_S \end{pmatrix} \\ - \underbrace{\begin{pmatrix} \frac{T_1 \Delta v}{v^2} & 0 \\ 0 & \frac{T_2 \Delta v_S}{v_S^2} \end{pmatrix}}_{\text{vanishes}}. \end{aligned} \quad (24)$$

The last term in Eq. (24) vanishes, because after the shift the tadpole conditions can be applied again. The mass matrix can now be rotated into the mass basis and all counterterm shifts can be applied leading to

$$\begin{aligned} D_{hh}^2 &= R_\alpha \mathcal{M} R_\alpha^T \rightarrow D_{hh}^2 + \begin{pmatrix} \delta m_{h_1}^2 & 0 \\ 0 & \delta m_{h_2}^2 \end{pmatrix} \\ &+ R_\alpha \begin{pmatrix} \frac{\delta T_1}{v} + v \Delta v \lambda & \frac{\delta_2}{2} (\Delta v v_S + v \Delta v_S) \\ \frac{\delta_2}{2} (\Delta v v_S + v \Delta v_S) & \frac{\delta T_2}{v_S} + d_2 v_S \Delta v_S \end{pmatrix} R_\alpha^T \\ &\equiv D_{hh}^2 + \begin{pmatrix} \delta m_{h_1}^2 & 0 \\ 0 & \delta m_{h_2}^2 \end{pmatrix} + \begin{pmatrix} \Delta D_{h_1 h_1}^2 & \Delta D_{h_1 h_2}^2 \\ \Delta D_{h_2 h_1}^2 & \Delta D_{h_2 h_2}^2 \end{pmatrix}. \end{aligned} \quad (25)$$

Using Eqs. (22) and (23) as well as the relations Eq. (11) between the potential parameters and the input parameters we can express the shifts $\Delta D_{h_i h_j}^2$ ($i, j = 1, 2$) as

$$\Delta D_{h_1 h_1}^2 = i(-i\lambda_{h_1 h_1 h_1}) \frac{-i}{m_{h_1}^2} i\delta T_{h_1} + i(-i\lambda_{h_1 h_1 h_2}) \frac{-i}{m_{h_2}^2} i\delta T_{h_2}, \quad (26a)$$

$$\Delta D_{h_1 h_2}^2 = i(-i\lambda_{h_1 h_1 h_2}) \frac{-i}{m_{h_1}^2} i\delta T_{h_1} + i(-i\lambda_{h_1 h_2 h_2}) \frac{-i}{m_{h_2}^2} i\delta T_{h_2}, \quad (26b)$$

$$\Delta D_{h_2 h_2}^2 = i(-i\lambda_{h_1 h_2 h_2}) \frac{-i}{m_{h_1}^2} i\delta T_{h_1} + i(-i\lambda_{h_2 h_2 h_2}) \frac{-i}{m_{h_2}^2} i\delta T_{h_2}, \quad (26c)$$

with the trilinear Higgs couplings given by

$$\lambda_{h_1 h_1 h_1} = 3m_{h_1}^2 \frac{v_S c_\alpha^3 + v_S^3}{v v_S}, \quad (27a)$$

$$\lambda_{h_1 h_1 h_2} = \frac{(2m_{h_1}^2 + m_{h_2}^2) s_\alpha c_\alpha (v_S c_\alpha - v_S^3)}{v v_S}, \quad (27b)$$

$$\lambda_{h_1 h_2 h_2} = \frac{(m_{h_1}^2 + 2m_{h_2}^2) s_\alpha c_\alpha (v_S c_\alpha + v_S^3)}{v v_S}, \quad (27c)$$

$$\lambda_{h_2 h_2 h_2} = 3m_{h_2}^2 \frac{v_S c_\alpha^3 - v_S^3}{v v_S}. \quad (27d)$$

In terms of Feynman diagrams this can be seen as the contribution of the tadpole diagram (times a factor i , at vanishing momentum transfer) to the propagators of h_1 and h_2 , which were not included previously in the definition of the self-energies. We define

$$i\Sigma_{h_i h_j}^{\text{tad}}(p^2) \equiv i\Sigma_{h_i h_j}(p^2) - i\Delta D_{h_i h_j}^2, \quad (28)$$

and the renormalized self-energies take the form

$$\begin{aligned} \hat{\Sigma}_{h_i h_j}(p^2) &= \Sigma_{h_i h_j}^{\text{tad}}(p^2) - \begin{pmatrix} \delta m_{h_1}^2 & 0 \\ 0 & \delta m_{h_2}^2 \end{pmatrix} \\ &+ \frac{\delta Z_{h_i h_j}^\dagger}{2} \left(p^2 \delta_{h_i h_j} - D_{h_i h_j}^2 \right) \\ &+ \left(p^2 \delta_{h_i h_j} - D_{h_i h_j}^2 \right) \frac{\delta Z_{h_i h_j}}{2}. \end{aligned} \quad (29)$$

This shift of contributions from the mass counterterm matrix into the self-energy corresponds to the inclusion of the tadpole diagrams into the self-energy. With this change in the renormalized self-energy the following results for the counterterms hold:

$$\delta m_{h_i}^2 = \text{Re}(\Sigma_{h_i h_i}^{\text{tad}}(m_{h_i}^2)), \quad (30a)$$

$$\delta Z_{h_i h_i} = -\text{Re} \left(\left. \frac{\partial \Sigma_{h_i h_i}^{\text{tad}}(p^2)}{\partial p^2} \right|_{p^2=m_{h_i}^2} \right), \quad (30b)$$

$$\delta Z_{h_i h_j} = \frac{2}{m_{h_i}^2 - m_{h_j}^2} \text{Re}(\Sigma_{h_i h_j}^{\text{tad}}(m_{h_j}^2)) \quad (i \neq j). \quad (30c)$$

Following a similar reasoning, the counterterms of the field A can be expressed as

$$\delta m_A^2 = \text{Re}(\Sigma_A^{\text{tad}}(m_A^2)), \quad (31)$$

$$\delta Z_A = -\text{Re} \left(\left. \frac{\partial \Sigma_A^{\text{tad}}(p^2)}{\partial p^2} \right|_{p^2=m_A^2} \right). \quad (32)$$

C. Renormalization of the mixing angle α

There are two parameters left to be renormalized. We start with the rotation angle α . Previous works [6,17] lead us to the conclusion that a scheme that is simultaneously stable (in the sense that the NLO corrections do not become unreasonably large) and gauge independent can be built by combining the one proposed in Refs. [19,20] with the gauge dependence handled by the use of the pinch technique [21,22]. The scheme proposed in [19,20] introduces a shift in α , the angle from the rotation matrix R_α ,

$$R_{\alpha,0} \approx R_{\delta\alpha} R_\alpha, \quad (33)$$

and by relating it to the field renormalization matrix constant leads to the following counterterm for α :

$$\delta\alpha = \frac{\delta Z_{h_1 h_2} - \delta Z_{h_2 h_1}}{4}. \quad (34)$$

The result is model independent, and it only assumes the mixing of solely two fields. This relation can now be expressed in terms of self-energies as

$$\delta\alpha = \frac{1}{2(m_{h_1}^2 - m_{h_2}^2)} \text{Re}(\Sigma_{h_1 h_2}^{\text{tad}}(m_{h_1}^2) + \Sigma_{h_1 h_2}^{\text{tad}}(m_{h_2}^2)). \quad (35)$$

This counterterm turns out to be gauge dependent. This in itself would not be a problem if the complete amplitude for the process was gauge independent, which is not the case. There is, however, a procedure to isolate this gauge dependence in a systematic and consistent way known as the pinch technique [21–24]. After successfully applying the pinch technique, the pinched self-energies can be defined by adding the additional contributions to the self-energies from the pinch technique. This results in

$$\begin{aligned}
i\Sigma_{h_i h_j}^{\text{pinch}}(p^2) &= i\Sigma_{h_i h_j}^{\text{tad}}(p^2) + i\Sigma_{h_i h_j}^{\text{add}}(p^2) \\
&= i\Sigma_{h_i h_j}^{\text{tad}}(p^2)|_{\{\xi=1\}} \\
&\quad + \frac{-ig^2}{32\pi^2 c_w^2} \left(p^2 - \frac{m_{h_i}^2 + m_{h_j}^2}{2} \right) O_{ij} B_0(q^2, m_Z^2, m_W^2) \\
&\quad + \frac{-ig^2}{16\pi^2} \left(p^2 - \frac{m_{h_i}^2 + m_{h_j}^2}{2} \right) O_{ij} B_0(q^2, m_W^2, m_W^2).
\end{aligned} \tag{36}$$

The loop integral B_0 and the factor O_{ij} as well as $\Sigma_{h_i h_j}^{\text{add}}(p^2)$ are defined in Appendix A. Note that the expression with $\xi = 1$ does not mean that a specific gauge has been chosen. The additional terms together with the tadpole self-energies result in a gauge-independent result which can just be written in that form. We can now define a gauge-independent counterterm for α , for which two different scales will be chosen:

- (i) Setting the external momenta to the respective On-shell (OS) masses, $p^2 = m_{h_i}^2$, called the OS pinched scheme.
- (ii) Setting the external momenta to the mean of the masses, $p^2 = p_*^2 = \frac{m_{h_1}^2 + m_{h_2}^2}{2}$, called the p^* pinched scheme.

In the p^* pinched scheme the additional gauge-independent terms from the pinch technique vanish so that the expression for the mixing angle counterterm becomes more compact. We can write the counterterm for α in the p_* scheme and the OS pinched scheme as

$$\delta\alpha_{p^*} = \frac{1}{(m_{h_1}^2 - m_{h_2}^2)} \text{Re} \left(\Sigma_{h_1 h_2}^{\text{tad}}(p_*^2) |_{\{\xi=1\}} \right), \tag{37a}$$

$$\delta\alpha_{\text{OS}} = \frac{1}{2(m_{h_1}^2 - m_{h_2}^2)} \text{Re} \left(\Sigma_{h_1 h_2}^{\text{pinch}}(m_{h_1}^2) + \Sigma_{h_1 h_2}^{\text{pinch}}(m_{h_2}^2) \right). \tag{37b}$$

With these definitions, $\delta\alpha$ is gauge independent by construction and the problem with the gauge dependence is solved.

D. Renormalization of v_S

The last parameter to be renormalized is the VEV v_S of the scalar singlet. We will be using a process-dependent scheme and also a derivation thereof where the conditions are imposed at the amplitude and not at the physical process level, defined as the zero external momentum (ZEM) scheme [6]. The latter, although less stable, allows one to cover the entire parameter space because it is not constrained by kinematic restrictions.

1. Process-dependent scheme

The process to be used needs a coupling constant proportional to v_S , and if we want to use a decay, the only possibilities in the CxSM are $h_1 \rightarrow AA$, $h_2 \rightarrow AA$, and $h_2 \rightarrow h_1 h_1$. Since we are interested in the Higgs decay into DM, the mass m_A is already constrained to be light enough for this decay to be allowed. If h_1 is the 125 GeV Higgs, the process $h_2 \rightarrow AA$ would not further constrain the parameter space, whereas the process $h_2 \rightarrow h_1 h_1$ would additionally reduce the allowed parameter space. Therefore one of the processes $h_i \rightarrow AA$ will be used to extract the singlet VEV renormalization constant, and because we want to use the measurement of the SM-like Higgs invisible width, the second Higgs will be used for that purpose. Note, however, that any of the two Higgs bosons can be the SM-like one, while the other can be either lighter or heavier than 125 GeV. Hence, there are two scenarios to be analyzed, and we have to find v_S for both.

In the process-dependent scheme the counterterm is calculated by forcing

$$\Gamma_{h_i \rightarrow AA}^{\text{LO}} = \Gamma_{h_i \rightarrow AA}^{\text{NLO}}; \tag{38}$$

that is, the LO and NLO decay widths are equal. This in turn leads to

$$0 = \text{Re} \left((\mathcal{A}_{h_i \rightarrow AA}^{\text{LO}})^* \mathcal{A}_{h_i \rightarrow AA}^{\text{NLO}} \right), \tag{39}$$

where $\mathcal{A}_{h_i \rightarrow AA}^{\text{LO}}$ is the amplitude of the process $h_i \rightarrow AA$ at LO and $\mathcal{A}_{h_i \rightarrow AA}^{\text{NLO}}$ is the amplitude at NLO. Because the LO amplitude is just a coupling constant, the expression further simplifies to

$$0 = \text{Re} \left(\mathcal{A}_{h_i \rightarrow AA}^{\text{NLO}} \right). \tag{40}$$

The NLO contribution $\mathcal{A}_{h_i \rightarrow AA}^{\text{NLO}}$ can be written in terms of the vertex corrections $\mathcal{A}_{h_i \rightarrow AA}^{\text{VC}}$ and the vertex counterterm such that

$$\begin{aligned}
0 &= \text{Re} \left(\mathcal{A}_{h_i \rightarrow AA}^{\text{NLO}} \right) \\
&= \text{Re} \left(\mathcal{A}_{h_i \rightarrow AA}^{\text{VC}} \right) \\
&\quad - \lambda_{h_i AA} \left(\frac{\delta\lambda_{h_i AA}}{\lambda_{h_i AA}} + \delta Z_A + \frac{\delta Z_{h_i h_i}}{2} + \frac{\lambda_{h_i AA}}{\lambda_{h_i AA}} \frac{\delta Z_{h_i h_i}}{2} \right),
\end{aligned} \tag{41}$$

where $i, j \in \{1, 2\}$, but $i \neq j$. And with the trilinear h_i couplings to the DM particles $\lambda_{h_i AA}$ given in Eq. (12) we have

$$\frac{\delta\lambda_{h_i AA}}{\lambda_{h_i AA}} = \frac{\delta m_{h_i}^2}{m_{h_i}^2} - \frac{\delta v_S}{v_S} + T_i(\alpha) \delta\alpha, \quad T_i(\alpha) \equiv \begin{cases} \cot \alpha, & i = 1 \\ -\tan \alpha, & i = 2 \end{cases}. \tag{42}$$

Finally, the expression for the counterterm v_S reads

$$\delta v_S^{h_1 \rightarrow AA} = v_S \left(-\text{Re} \left(\frac{\mathcal{A}_{h_1 \rightarrow AA}^{\text{VC}}}{\lambda_{h_1 AA}} \right) + \frac{\delta m_{h_1}^2}{m_{h_1}^2} + \cot \alpha \delta \alpha + \delta Z_A \right. \\ \left. + \frac{\delta Z_{h_1 h_1}}{2} + \frac{\lambda_{h_2 AA}}{\lambda_{h_1 AA}} \frac{\delta Z_{h_2 h_1}}{2} \right), \quad (43a)$$

$$\delta v_S^{h_2 \rightarrow AA} = v_S \left(-\text{Re} \left(\frac{\mathcal{A}_{h_2 \rightarrow AA}^{\text{VC}}}{\lambda_{h_2 AA}} \right) + \frac{\delta m_{h_2}^2}{m_{h_2}^2} - \tan \alpha \delta \alpha + \delta Z_A \right. \\ \left. + \frac{\delta Z_{h_2 h_2}}{2} + \frac{\lambda_{h_1 AA}}{\lambda_{h_2 AA}} \frac{\delta Z_{h_1 h_2}}{2} \right), \quad (43b)$$

for the two processes. These counterterms are gauge independent and lead to UV-finite results. The renormalization scheme also leads to stable results. Therefore, the only drawback is the kinematic restriction

$$m_{h_i} > 2m_A, \quad (44)$$

which forces us to be in a restricted region of the parameter space. We discuss a solution to avoid this restriction in the next section.

2. ZEM scheme

The ZEM scheme was introduced in [6] to avoid kinematic restrictions on the parameter space, and we will now apply it to the CxSM. It is a simple derivation of the process-dependent scheme, where the square of all external momenta are set to zero at the level of the amplitude,

$$p_{\text{in}}^2 = p_{\text{out1}}^2 = p_{\text{out2}}^2 = 0, \quad (45)$$

eliminating therefore the kinematic constraint. Choosing the same physical processes, the condition now reads

$$0 = \text{Re}(\mathcal{A}_{h_i \rightarrow AA}^{\text{NLO}}(\{p^2 = 0\})), \quad (46)$$

where $p^2 = 0$ means that all squared external momenta are set to zero. There is another difference relative to the process-dependent scheme: the NLO leg corrections are not canceled by the corresponding counterterms, because the leg counterterms are defined through the OS scheme. Therefore Eq. (46) now takes the form

$$0 = \text{Re}(\mathcal{A}_{\text{VC}}^{h_i \rightarrow AA}(\{p^2 = 0\}) + \mathcal{A}_{\text{Leg}}^{h_i \rightarrow AA}(\{p^2 = 0\})) \\ + \lambda_{h_i AA} \left(-\frac{\delta \lambda_{h_i AA}}{\lambda_{h_i AA}} + \delta Z_A + \frac{\delta Z_{h_i h_i}}{2} + \frac{\delta m_{h_i}^2}{m_{h_i}^2} \right. \\ \left. + \frac{2\delta m_A^2}{m_A^2} + \frac{\lambda_{h_j AA}}{\lambda_{h_i AA}} \frac{m_{h_i}^2}{m_{h_j}^2} \frac{\delta Z_{h_i h_j}}{2} \right). \quad (47)$$

Again, this equation can be solved for the two processes $h_1 \rightarrow AA$ and $h_2 \rightarrow AA$ to obtain the counterterms

$$\delta v_S^{\text{ZEM}, h_1 \rightarrow AA} \\ = v_S \left(-\text{Re} \left(\frac{\mathcal{A}_{\text{VC}}^{h_1 \rightarrow AA}(\{p^2 = 0\}) + \mathcal{A}_{\text{Leg}}^{h_1 \rightarrow AA}(\{p^2 = 0\})}{\lambda_{h_1 AA}} \right) \right. \\ \left. + \cot \alpha \delta \alpha - \delta Z_A - \frac{2\delta m_A^2}{m_A^2} - \frac{\delta Z_{h_1 h_1}}{2} - \cot \alpha \frac{\delta Z_{h_1 h_2}}{2} \right), \quad (48a)$$

$$\delta v_S^{\text{ZEM}, h_2 \rightarrow AA} \\ = v_S \left(-\text{Re} \left(\frac{\mathcal{A}_{\text{VC}}^{h_2 \rightarrow AA}(\{p^2 = 0\}) + \mathcal{A}_{\text{Leg}}^{h_2 \rightarrow AA}(\{p^2 = 0\})}{\lambda_{h_2 AA}} \right) \right. \\ \left. - \tan \alpha \delta \alpha - \delta Z_A - \frac{2\delta m_A^2}{m_A^2} - \frac{\delta Z_{h_2 h_2}}{2} - \tan \alpha \frac{\delta Z_{h_2 h_1}}{2} \right). \quad (48b)$$

We now just have to check if the final result is finite and gauge independent. The question of gauge dependence in the alternative tadpole scheme is always related to wave function renormalization constants. A thorough analysis leads to the conclusion that although finite the result is gauge dependent due to the term

$$\frac{\delta Z_{h_i h_i}}{2} + \frac{\lambda_j m_{h_i}^2}{\lambda_i m_{h_j}^2} \frac{\delta Z_{h_i h_j}}{2}, \quad (49)$$

for the corresponding process $h_i \rightarrow AA$. The problem was solved by simply replacing the self-energies in the wave function renormalization constants in Eq. (48) by their pinched versions. This way δv_S becomes gauge independent. This change in the $\delta Z_{h_i h_j}$, however, is applied only to terms appearing in Eq. (48) where the ZEM counterterm of v_S is defined and not anywhere else. Otherwise, a gauge dependence in the overall amplitude of the renormalized process could be reintroduced. Therefore, the resulting counterterms for v_S in this modified ZEM scheme read

$$\delta v_S^{\text{ZEMGI}, h_1 \rightarrow AA} \\ = v_S \left(-\text{Re} \left(\frac{\mathcal{A}_{\text{VC}}^{h_1 \rightarrow AA}(\{p^2 = 0\}) + \mathcal{A}_{\text{Leg}}^{h_1 \rightarrow AA}(\{p^2 = 0\})}{\lambda_{h_1 AA}} \right) \right. \\ \left. + \cot \alpha \delta \alpha - \delta Z_A - \frac{2\delta m_A^2}{m_A^2} - \frac{\delta Z_{h_1 h_1}^{\text{pinched}}}{2} - \cot \alpha \frac{\delta Z_{h_1 h_2}^{\text{pinched}}}{2} \right), \quad (50a)$$

$$\begin{aligned}
& \delta v_S^{\text{ZEMGI}, h_2 \rightarrow AA} \\
&= v_S \left(-\text{Re} \left(\frac{\mathcal{A}_{\text{VC}}^{h_2 \rightarrow AA}(\{p^2 = 0\}) + \mathcal{A}_{\text{Leg}}^{h_2 \rightarrow AA}(\{p^2 = 0\})}{\lambda_{h_2 AA}} \right) \right. \\
&\quad \left. - \tan \alpha \delta \alpha - \delta Z_A - \frac{2\delta m_A^2}{m_A^2} - \frac{\delta Z_{h_2 h_2}^{\text{pinched}}}{2} - \tan \alpha \frac{\delta Z_{h_2 h_1}^{\text{pinched}}}{2} \right). \quad (50b)
\end{aligned}$$

The renormalization is now complete, and before moving to the presentation of the NLO results we will discuss the constraints imposed on the model.

IV. CONSTRAINTS ON THE MODEL

The constraints imposed to find the allowed parameter space are implemented in SCANNERS [25–27]. In this section we will just briefly review the most relevant theoretical and experimental constraints considered.

A. Theoretical constraints

- (i) *Boundedness from below* The conditions to have a stable minimum are easily obtained by writing $\Phi^\dagger \Phi \equiv x$ and $|\mathbb{S}|^2 \equiv y$ and by writing the quartic terms of the potential

$$\begin{aligned}
V_{\text{quartic}}(x, y) &= \frac{\lambda}{4} x^2 + \frac{\delta_2}{2} xy + \frac{d_2}{4} y^2 \\
&= \frac{1}{4} \begin{pmatrix} x & y \end{pmatrix}^T \begin{pmatrix} \lambda & \delta_2 \\ \delta_2 & d_2 \end{pmatrix} \begin{pmatrix} x \\ y \end{pmatrix}. \quad (51)
\end{aligned}$$

Forcing the potential to be bounded in all directions leads to the following conditions at tree level:

$$\lambda > 0 \wedge d_2 > 0 \wedge (\delta_2^2 < \lambda d_2 \quad \text{if } \delta_2 < 0). \quad (52)$$

- (ii) *Perturbative unitarity constraints* Following [28] we force the eigenvalues of the scattering matrix $\mathcal{M}_{2 \rightarrow 2}$ of all possible two-to-two scalar scattering interactions to obey

$$|\lambda_i| < 8\pi, \quad (53)$$

leading to

$$\begin{aligned}
& |\lambda| \leq 16\pi \wedge |d_2| \leq 16\pi \wedge |\delta_2| \leq 16\pi, \\
& \wedge \left| \frac{3}{2}\lambda + d_2 \pm \sqrt{\left(\frac{3}{2}\lambda - d_2\right)^2 + 2\delta_2^2} \right| \leq 16\pi. \quad (54)
\end{aligned}$$

- (iii) *Stability of the vacuum* In the CxSM the most general vacuum structure is obtained by the following expectation values for the fields:

$$\langle \Phi \rangle = \frac{1}{\sqrt{2}} \begin{pmatrix} 0 \\ v \end{pmatrix}, \quad \langle \mathbb{S} \rangle = \frac{1}{\sqrt{2}} (v_S + i v_A), \quad (55)$$

because of the $SU(2)$ invariance. Therefore, the value of the tree-level potential at each vacuum configuration is given by $V(v, v_S, v_A)$. We have chosen to work in the configuration where the potential is $V(v, v_S, 0)$ to have one DM candidate. In Appendix B we show that by choosing the vacuum configuration with nonzero v and v_S (and $v_A = 0$) to be a minimum automatically implies that this configuration is the absolute minimum at tree level.

B. Experimental constraints

Before moving to the experimental constraints we note that $\rho = m_W^2 / (m_Z^2 c_w^2)$ where $m_{W,Z}$ are the masses of the massive W and Z bosons, respectively, and c_w denotes the cosine of the Weinberg angle, is equal to 1 at tree level, as in the SM. Also, no tree-level flavor-changing neutral currents are introduced because the gauge singlet does not couple to fermions and to gauge bosons in the gauge basis.

We will now briefly review the experimental constraints implemented in SCANNERS and used for the generation of parameter points.

- (i) *S, T, U precision parameters* The additional scalar fields in the CxSM contribute to the gauge bosons self-energies, and this implies deviations from the SM predictions. These deviations relative to the SM have to be within experimental bounds, i.e., SCANNERS compares the model predictions with the electroweak precision results from experiment. Then the program applies a consistency check on the S, T, U parameters [29] with 95% confidence level to check if the constraints are fulfilled.
- (ii) *Compatibility with the LHC Higgs data and exclusion bounds* There are two important constraints coming from colliders. The most relevant one is the one coming from the LHC related to the measurements of the discovered Higgs boson. The searches for additional scalars also play a role in restricting the parameter space of the model. SCANNERS enforces these bounds by the interfaces with HiggsSignals [30,31] and HiggsBounds [32,33]. Agreement of the signal rates of the SM-like Higgs boson of the CxSM with the observations at 2σ level is checked by HiggsSignals-2.6.1. Through HiggsBounds-5.9.0 the exclusion bounds from searches for extra scalars are taken into account.
- (iii) *DM relic density* The CxSM has a scalar DM candidate, and therefore the predicted DM relic density of this model should not exceed the measured value. Smaller values are not excluded since they allow for additional contributions coming from other sources. SCANNERS is interfaced with the

program package MicrOMEGAs [34] to include this constraint from the relic density.

- (iv) *DM direct detection* As previously stated, the DM-nucleon cross section is only relevant at one-loop order due to a cancellation that renders the tree-level cross section proportional to the DM velocity and therefore negligible [7,8]. However, one-loop corrections to the DM-nucleon spin-independent cross section have to be below the present experimentally measured result from XENON1T [11], as discussed in [9,10]. We will come back to this important constraint in the next section.

V. RESULTS AND DISCUSSION

A. Higgs decay into dark matter

The CxSM has two CP -even scalars h_1 or h_2 and any of them can play the role of the 125 GeV SM-like Higgs boson denoted h_{125} in the following. The non SM-like Higgs can be either heavier or lighter than 125 GeV. To optimize the analysis we fixed h_1 to always be the lightest of the two and considered two distinct scenarios:

- (i) $m_{h_1} = m_{h_{125}}$ (scenario I): the width is calculated from $h_1 \rightarrow AA$ and the process $h_2 \rightarrow AA$ is chosen for the renormalization of v_S .
- (ii) $m_{h_2} = m_{h_{125}}$ (scenario II): the width is calculated from $h_2 \rightarrow AA$ and the process $h_1 \rightarrow AA$ is chosen for the renormalization of v_S .

We now proceed to the calculation of the 125 GeV Higgs partial decay width into two DM particles at electroweak NLO. The calculations of the NLO corrections were performed using FeynRules 2.3.35 [35–37], FeynArts 3.10 [38,39], and FeynCalc 9.3.1 [40,41]. Loop integrals were computed using LoopTools [42,43]. The model file was independently generated using SARAH 4.14.2 [44–48]. We performed two independent calculations and found agreement between both results.

The LO decay width is given by

$$\Gamma_{h_{125} \rightarrow AA}^{\text{LO}} = \frac{\lambda(m_{h_{125}}^2, m_A^2, m_A^2)}{32\pi m_{h_{125}}^3} |\mathcal{A}_{h_{125} \rightarrow AA}^{\text{LO}}|^2, \quad (56)$$

while the NLO expression can be written as

$$\Gamma_{h_{125} \rightarrow AA}^{\text{NLO}} = \frac{\lambda(m_{h_{125}}^2, m_A^2, m_A^2)}{32\pi m_{h_{125}}^3} \left(|\mathcal{A}_{h_{125} \rightarrow AA}^{\text{LO}}|^2 + 2\text{Re}\left((\mathcal{A}_{h_{125} \rightarrow AA}^{\text{LO}})^* \mathcal{A}_{h_{125} \rightarrow AA}^{\text{NLO}} \right) \right), \quad (57)$$

with $\lambda(x, y, z) = x^2 + y^2 + z^2 - 2xy - 2xz - 2yz$ and \mathcal{A}^{LO} and \mathcal{A}^{NLO} denoting the LO and NLO amplitudes, respectively.

The LO amplitude is simply the coupling constant

$$i\mathcal{A}_{h_i \rightarrow AA}^{\text{LO}} = -i\lambda_{h_i AA}, \quad (58)$$

and therefore the decay width takes the form

$$\Gamma_{h_1 \rightarrow AA}^{\text{LO}} = \frac{s_\alpha^2 m_{h_1} \lambda(m_{h_1}^2, m_A^2, m_A^2)}{32\pi v_S^2}, \quad (59a)$$

$$\Gamma_{h_2 \rightarrow AA}^{\text{LO}} = \frac{c_\alpha^2 m_{h_2} \lambda(m_{h_2}^2, m_A^2, m_A^2)}{32\pi v_S^2}, \quad (59b)$$

where both h_1 and h_2 can be the SM-like Higgs h_{125} .

For the NLO amplitude we need to compute the vertex corrections together with the counterterm contributions. The vertex corrections are just the sum of all irreducible contributions at one-loop order while the vertex counterterm can be read off the Lagrangian yielding

$$\mathcal{A}_{h_i \rightarrow AA}^{\text{CT}} = -\lambda_{h_i AA} \left(\frac{\delta\lambda_{h_i AA}}{\lambda_{h_i AA}} + \delta Z_A + \frac{\delta Z_{h_i h_i}}{2} + \frac{\lambda_{h_i AA} \delta Z_{h_i h_i}}{\lambda_{h_i AA} 2} \right), \quad (60)$$

where $i, j \in \{1, 2\}$ but $i \neq j$. We finally arrive at the overall NLO contributions for the processes $h_i \rightarrow AA$,

$$\mathcal{A}_{h_1 \rightarrow AA}^{\text{NLO}} = \mathcal{A}_{h_1 \rightarrow AA}^{\text{VC}} - \lambda_{h_1 AA} \left(\frac{\delta m_{h_1}^2}{m_{h_1}^2} - \frac{\delta v_S}{v_S} + \cot\alpha \delta\alpha + \delta Z_A + \frac{\delta Z_{h_1 h_1}}{2} + \cot\alpha \frac{m_{h_2}^2 \delta Z_{h_2 h_1}}{m_{h_1}^2 2} \right), \quad (61a)$$

$$\mathcal{A}_{h_2 \rightarrow AA}^{\text{NLO}} = \mathcal{A}_{h_2 \rightarrow AA}^{\text{VC}} - \lambda_{h_2 AA} \left(\frac{\delta m_{h_2}^2}{m_{h_2}^2} - \frac{\delta v_S}{v_S} + \cot\alpha \delta\alpha + \delta Z_A + \frac{\delta Z_{h_2 h_2}}{2} + \tan\alpha \frac{m_{h_1}^2 \delta Z_{h_1 h_2}}{m_{h_2}^2 2} \right), \quad (61b)$$

which will be calculated numerically using Eq. (57). The value obtained for the width depends on the renormalization scheme used, which will be discussed in the next section. We have explicitly checked that for all scenarios the NLO width is UV-finite and gauge independent.

B. Allowed parameter space

For our numerical investigation we performed a scan in the CxSM parameter space using SCANNERS [25–27] and kept only those points that are compatible with the above described theoretical (calculated at LO) and experimental constraints. The scan ranges for the input parameters are summarized in Table I. The DM mass has to be below 62.5 GeV for $h_{125} \rightarrow AA$ to be kinematically allowed. The SM input parameters are taken from [49], and their values

TABLE I. The scan ranges used for the generation of parameter points with SCANNERS.

Parameter	Range	
	Lower	Upper
m_s	30 GeV	1000 GeV
m_A	10 GeV	62 GeV
v_S	1 GeV	1000 GeV
α	-1.57	1.57

TABLE II. The SM parameter values used in the numerical evaluation taken from [49].

SM parameter	Value
α	1/137
m_Z	91.1876 GeV
m_W	80.379 GeV
$m_{h_{125}}$	125.09 GeV
m_τ	1.777 GeV
m_b	4.7 GeV
m_t	172.5 GeV

are given in Table II. Note that all these parameters enter the calculation via the electroweak (EW) one-loop corrections.

We have also used the program BSMP [50,51] to check for the possibility of having a strong first order EW phase transition (SFOEWPT). We found that in the parameter space probed there were no points with a SFOEWPT. Before starting the discussion of the allowed parameter space we again remind the reader that there is a kinematical constraint that applies to the process-dependent scheme but not to the ZEM scheme of the counterterm δv_S .

As previously discussed, two of six parameters are fixed, one is by G_F and the other one is the 125 GeV Higgs boson mass. This leaves us with the four input parameters m_s, m_A, α, v_S where m_s denotes the scalar mass of the non-125 GeV Higgs boson. In Fig. 1 we show correlations between α, v_S , and m_s . In the upper row a strong correlation can be seen between α and v_S . This is to be expected since all SM couplings to the h_{125} Higgs boson have an additional c_α in scenario I or s_α in scenario II. These couplings are very well measured, and only small deviations are allowed. Thus, the additional factor has to be close to 1 and α has to be close to 0 or $\pm \frac{\pi}{2}$, respectively. Moreover, the parameters α and v_S are connected through the decay width

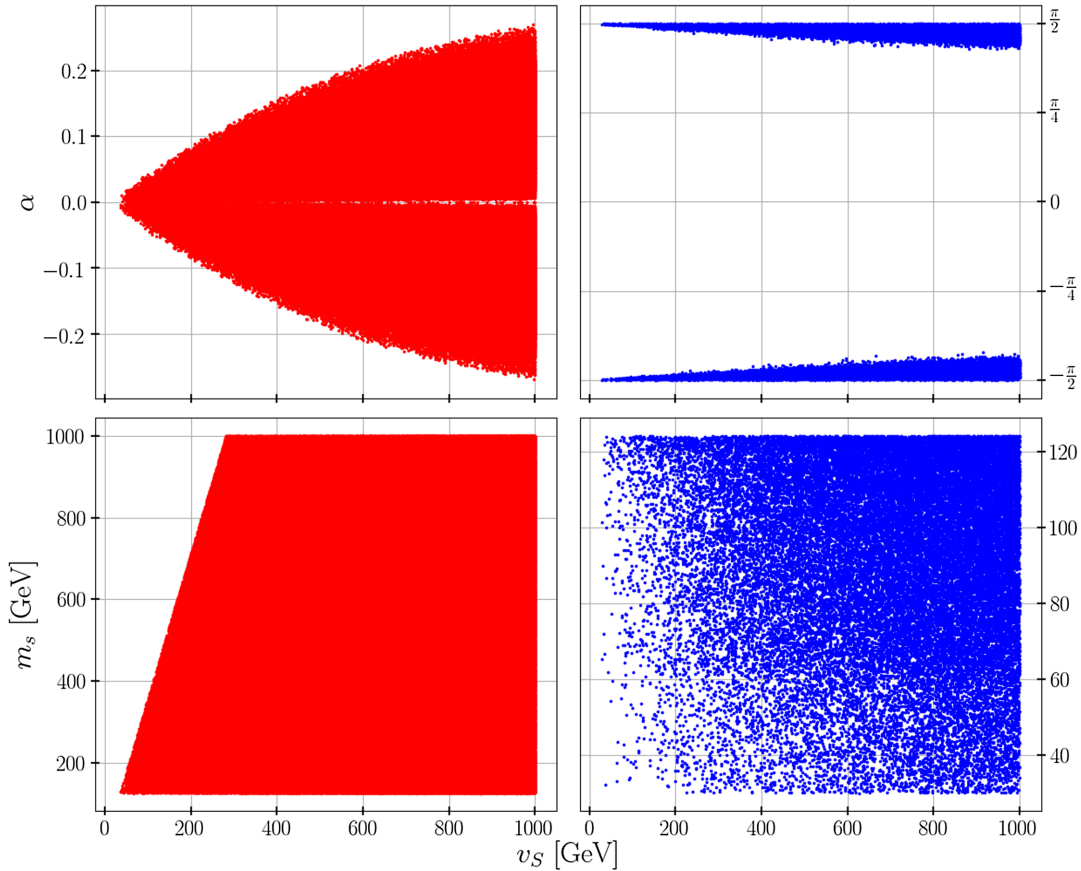


FIG. 1. Input parameters α vs v_S in the upper row and m_s vs v_S in the lower row. The red plots on the left side are for the scenario where the 125 GeV Higgs boson is the lighter scalar particle, and the blue plots on the right are for the heavier Higgs scenario.

of the 125 GeV Higgs boson into DM particles. As can be seen in Eq. (59), the LO decay width in scenario I is proportional to

$$\Gamma_{h_1 \rightarrow AA}^{\text{LO}} \propto \frac{s_\alpha^2}{v_S^2}. \quad (62)$$

Thus, in order for the LO branching ratio of the 125 GeV Higgs into DM particles in the CxSM not to exceed experimental limits [3], this ratio has to be small. Therefore, if v_S is small, α has to be small. This behavior can be seen in Fig. 1. In scenario II the LO decay width is proportional to

$$\Gamma_{h_2 \rightarrow AA}^{\text{LO}} \propto \frac{c_\alpha^2}{v_S^2}. \quad (63)$$

Therefore, if v_S is small, α has to be close to $\pm \frac{\pi}{2}$, which can be seen in Fig. 1 as well. One should also mention that there is a hard bound on α coming from the Higgs coupling measurements.

The plots in the lower row in Fig. 1 show the relation between v_S and m_s . The two parameters m_s and v_S can be related via d_2 . Because in scenario I $m_s = m_{h_2}$ and α cannot deviate much from zero, we can write

$$d_2 = \frac{m_{h_{125}}^2 + m_s^2 + \cos(2\alpha)(m_s^2 - m_{h_{125}}^2)}{v_S^2} \xrightarrow{\alpha \rightarrow 0} \frac{2m_s^2}{v_S^2}. \quad (64)$$

Using again the small angle approximation in Eq. (11), λ and δ_2 can be expressed as

$$\lambda \xrightarrow{\alpha \rightarrow 0} \frac{2m_{h_1}^2}{v^2} = \frac{2m_{h_{125}}^2}{v^2}, \quad (65)$$

$$\delta_2 \xrightarrow{\alpha \rightarrow 0} 0. \quad (66)$$

With these simplified expressions the fourth constraint in Eq. (54) results in

$$\left| \frac{3}{2}\lambda + d_2 \pm \left(\frac{3}{2}\lambda - d_2 \right) \right| \leq 16\pi$$

$$\Rightarrow d_2 \leq 8\pi \Rightarrow m_s \leq \sqrt{4\pi}v_S, \quad (67)$$

where d_2 was considered to be positive. This relation explains the line in Fig. 1 (lower left) for scenario I, showing m_s and v_S are linearly related with the correctly predicted slope. The same calculation applies to scenario II. In this case, $m_s = m_{h_1}$ and the angle α is close to $\pm \frac{\pi}{2}$. The conclusion is again that m_s and v_S are linearly related. For example, setting m_s to the highest possible value in this scenario, i.e., about 125 GeV, v_S has to be at least 35 GeV. In this scenario only a small part of the parameter space is constrained, but in Fig. 1 (right) we see that the far left side

of the plot indeed contains no parameter points in scenario II.

Figure 2 shows the parameter space spanned by m_s and m_A . The blue points (scenario II) are the ones where the kinematical constraint (due to the process-dependent scheme) appears. As expected the constraint is not there for scenario I (red points). In scenario I the DM mass m_A prefers values close to 125/2 GeV, whereas in scenario II (blue points), m_A has values close to half of m_s or also close to half of $m_{h_{125}}$ in the ZEM scheme where the kinematic constraint $2m_A < m_s$ from the renormalization condition on v_S ceases to apply. This behavior results from DM constraints applied on the DM mass m_A , with the dominant constraints coming from the relic density. To visualize the effect of DM constraints, we show in green the points that passed all constraints except the dark matter ones. The reason for these constraints is the requirement that the relic density obtained in the CxSM must not exceed the observed value of the relic density. Therefore, the thermal annihilation processes of two DM particles A into one of the scalar particles h_i must be efficient enough. This annihilation is enhanced close to the threshold, so that the DM mass m_A is preferably close to half of the 125 GeV or half of m_s .

In Fig. 3 (left) we present a histogram showing the points frequency as a function of the relic density for both scenarios. This plot clearly shows us that there are points that saturate the relic density but most of the points have a low $h^2\Omega_{cdm}$ and would need other DM candidates. The percentage of points that is in the range $-5\sigma < h^2\Omega_{cdm}^{cv} \leq 2\sigma$, where $h^2\Omega_{cdm}^{cv}$ is the experimental central value, is around 1% and the preferred values for the parameters are for the two resonant regions already discussed. In the right panel we present the relic density as a function of the DM mass with m_s presented by the color bar for the scenario where $m_{h_2} = 125$ GeV. There are points that saturate the relic density in the entire DM mass range probed. We clearly see that these points all have a DM mass that is half of m_s or half of m_{h_2} . There are also some outliers that saturate the relic density in the region where m_s is roughly between 30 and 50 GeV for a DM mass above 30 GeV. For the other scenario, since only the case half of 125 GeV is possible, all values of m_{h_2} can in principle saturate the relic density. Thus, the model is able to explain the observed relic density.

In Fig. 4 we show a histogram of the frequency of the variable α without and with the relic density constraint for scenario I. Without the DM constraints there is a bound on α that forces it to be close to zero. This is related to the already discussed bounds from colliders. The Boltzmann equation is given by

$$\frac{dn}{dt} + 3Hn = \langle \sigma v \rangle (n_{eq}^2 - n^2), \quad (68)$$

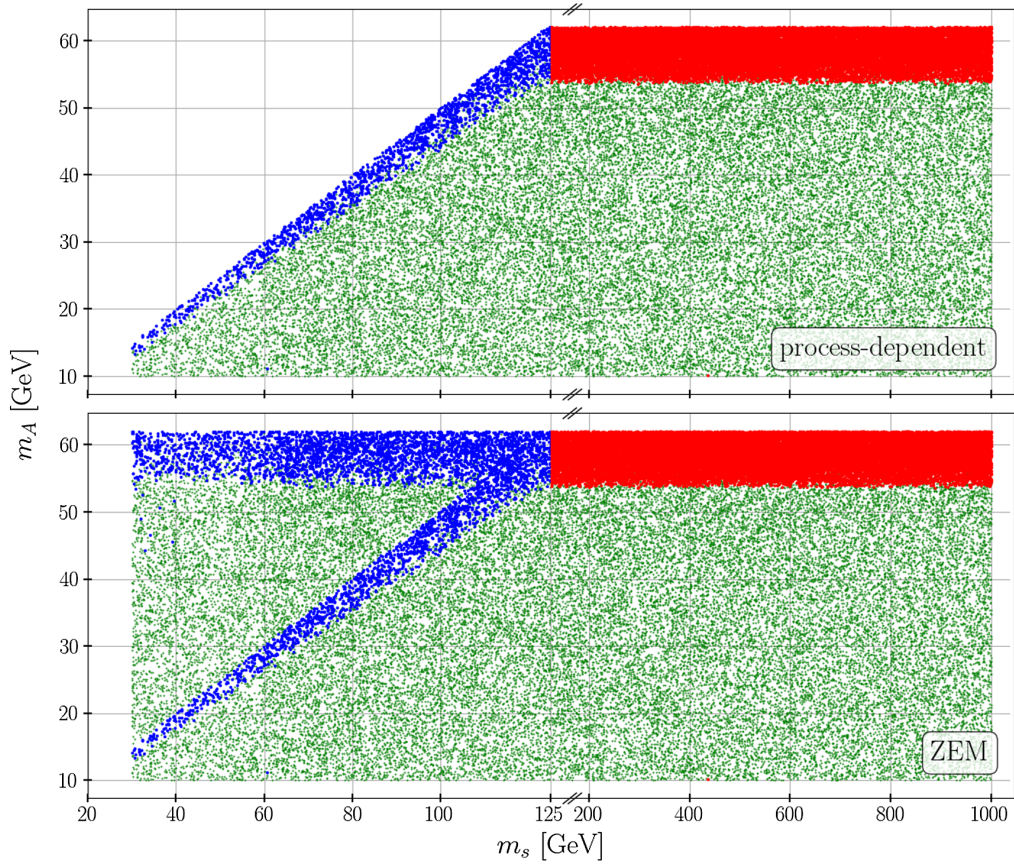


FIG. 2. m_A vs the non-125 GeV scalar mass m_s . The red points are for the scenario where the 125 GeV Higgs is the lighter scalar particle and the blue points the other scenario. The green points are parameter points rejected by DM constraints.

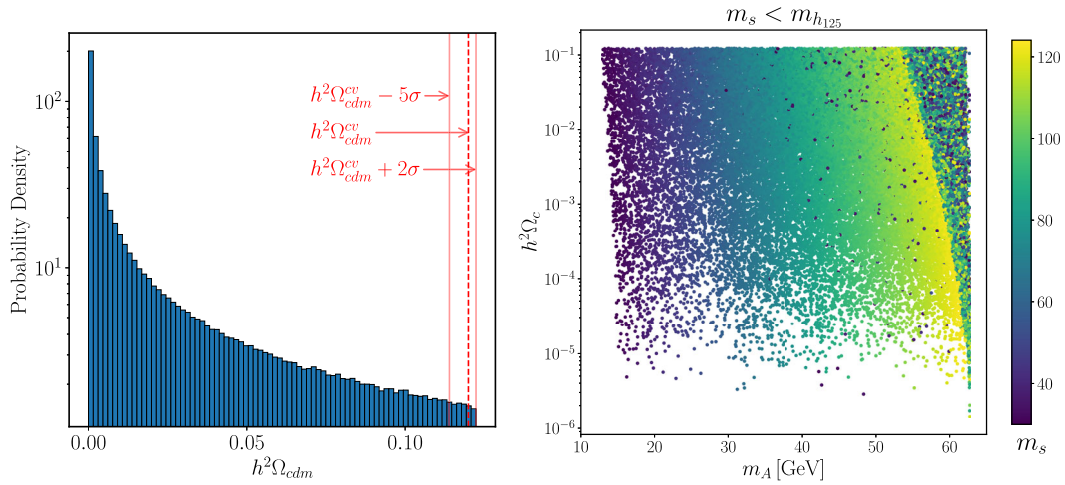


FIG. 3. Left: Histogram showing the points frequency as a function of the relic density. The vertical dashed line indicates the observed DM relic density and the superscript cv stands for central value. The other two vertical lines correspond to the bounds that we consider to saturate the relic density. Right: Relic density as a function of the DM mass with m_s presented by the color bar for the scenario where $m_{h_2} = 125$ GeV.

where n is the DM number density, H is the Hubble parameter, $\langle\sigma v\rangle$ is the velocity-averaged cross section, and n_{eq}^2 is the density of DM particles when in thermal

equilibrium with the photon bath. The annihilation cross section $\sigma(AA \rightarrow SMSM)$, where SM are SM particles, is proportional to $\sin\alpha\cos\alpha$. Hence, if either $\sin\alpha \rightarrow 0$ or

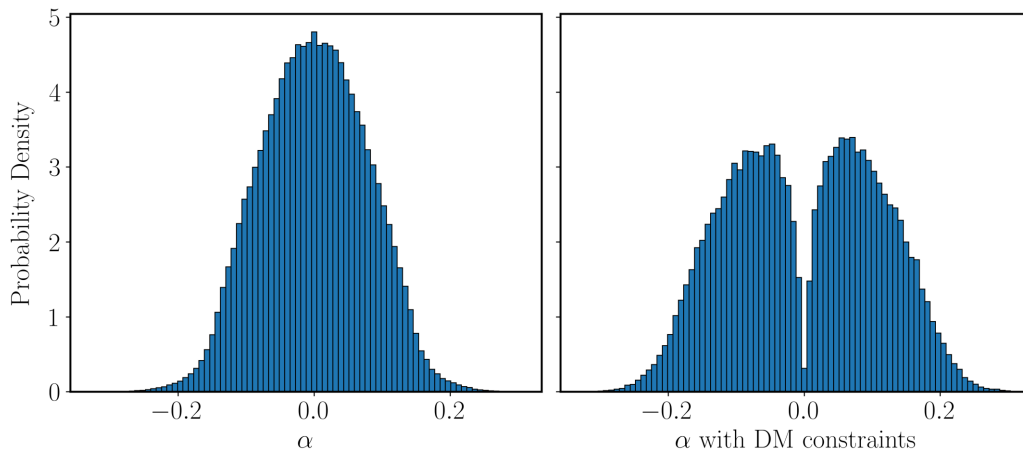


FIG. 4. Histogram of the frequency of the variable α without (left) and with (right) the relic density constraint for scenario I.

$\cos \alpha \rightarrow 0$, we get $\langle \sigma v \rangle \rightarrow 0$ and no freeze-out will occur or the relic density will be extremely high at the end of freeze-out.

The interesting feature is then that as we move closer to the limit where the couplings are all SM-like ($\alpha \approx 0$ is scenario I), we lose the DM candidate because of the constraints from DM. This is not surprising because in this limit the portal coupling δ_2 vanishes [compare with Eq. (11c)] and freeze-out is no longer possible.

We note that all parameters were sampled from a uniform distribution and no correlations have been imposed. Our goal is to show that, by sampling in this way, we see that there are regions which are preferred, such as those with a low DM relic density, and that there are strongly disfavored regions, such as the ones with the mixing angle α too close to zero.

Let us now move to the last constraint coming from DM, the direct detection process. Since we allow DM not to saturate the relic density, we need to define a DM fraction

$$f_{AA} = \frac{(\Omega h^2)_A}{(\Omega h^2)_{\text{DM}}^{\text{obs}}}, \quad (69)$$

where $(\Omega h^2)_A$ is the calculated relic density for each point in the CxSM and $(\Omega h^2)_{\text{DM}}^{\text{obs}}$ is the central value of the experimental measurement. In the comparison with the data, we are actually comparing an effective DM annihilation cross section defined by

$$\sigma_{\text{eff}} = f_{AA} \sigma_{AN}, \quad (70)$$

where f_{AA} and σ_{AN} , the direct detection DM nucleon cross section, are calculated by MicrOMEGAs. This is because the experimental limits assume the DM candidate to make up for all of the DM abundance.

This constraint is particularly relevant because it directly probes the portal coupling just as the invisible decay. Even if, as we have already discussed, the DM nucleon cross

section is only relevant at one-loop order, it could be that the experimental bound from XENON1T [11] would provide a stronger restriction than the one from the invisible Higgs decay. It turns out, however, that it does not. In Fig. 5 we present the effective spin-independent DM nucleon cross section [9,10] as a function of the DM mass for scenario I (left) and scenario II (right). The neutrino floor [52] is also presented as a gray shaded region. For the range of masses considered it is below a line of about 10^{-48} cm^2 . We can see that the points are not only below the XENON1T line but they are also below the neutrino floor and therefore have extremely small chances of being detected directly. Therefore, in the near future, and perhaps also in the far future, information about the dark sector of the CxSM will come only from the LHC. This shows the importance of taking into account the radiative corrections for the invisible Higgs decay.

C. Numerical results and analysis of the SM Higgs decay into DM

In the following, we present and discuss the LO and NLO decay widths for all allowed points in the parameter space, for the two scenarios. There are a total of four schemes corresponding to the combination of the choices of the counterterms $\delta\alpha$ (p^* pinched and OS pinched) and δv_S (process dependent and ZEM). We display results for the relative size of the NLO decay width with respect to the LO result, defined as

$$\Delta\Gamma \equiv \frac{\Gamma_{h_{125} \rightarrow AA}^{\text{NLO}}}{\Gamma_{h_{125} \rightarrow AA}^{\text{LO}}} - 1 = \frac{2\text{Re}(\mathcal{A}_{h_{125} \rightarrow AA}^{\text{NLO}})}{\mathcal{A}_{h_{125} \rightarrow AA}^{\text{LO}}}. \quad (71)$$

In Fig. 6 we present $\Delta\Gamma$ as a function of m_s for the two scenarios and for the four different possible combinations of renormalization conditions. The relative NLO corrections in scenario II (blue points) are quite small in the process-dependent scheme (denoted by “pd” in the plot),

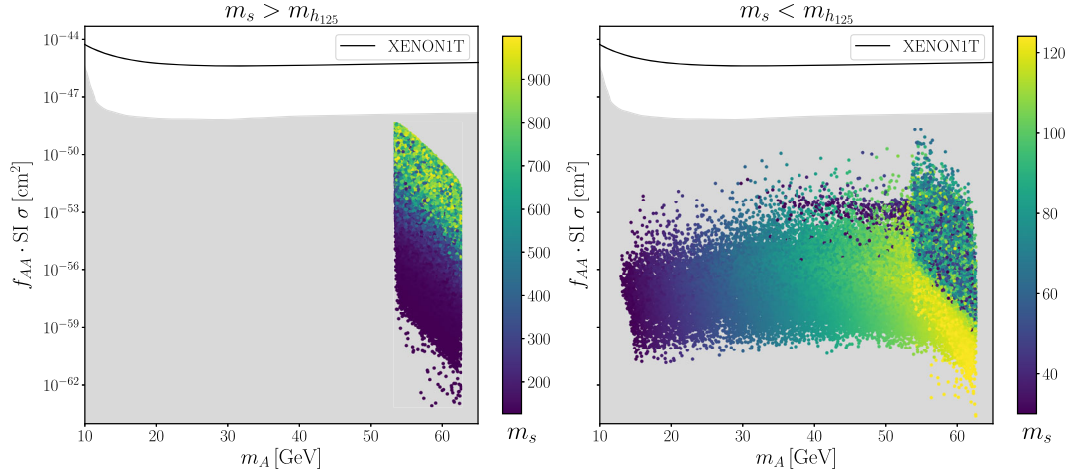


FIG. 5. Effective spin independent nucleon DM cross section as a function of the DM mass for scenario I (left) and scenario II (right). Also shown is the XENON1T [11] exclusion line (black line). The gray shaded region corresponds to the neutrino floor.

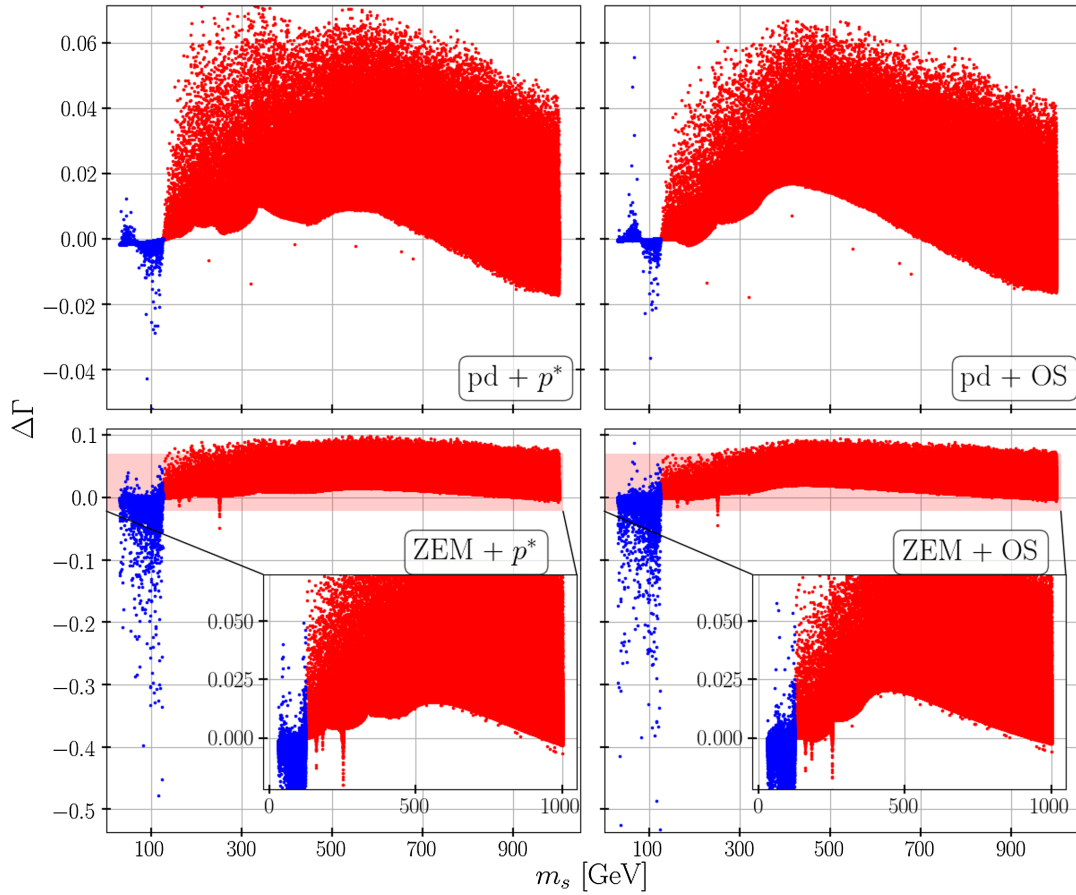


FIG. 6. $\Delta\Gamma$ plotted against the scalar mass m_s , where $h_{125} = h_1$ (red points) and $h_{125} = h_2$ (blue points). All different combinations of possible renormalization schemes are shown. Interesting sections (indicated by the red band) of the two plots in the second row are also shown in more detail.

but become comparatively large in the ZEM scheme with respect to scenario I (red points). Both in scenario I and in scenario II, $\Delta\Gamma$ is barely affected by the choice of the renormalization scheme of α . Larger differences occur

when changing the renormalization scheme of v_s from the process-dependent to the ZEM scheme, but they still remain relatively stable, i.e., of $\mathcal{O}(1\%)$, in scenario I. Note, that the peaks in scenario I in the ZEM scheme that induce

larger $\Delta\Gamma$ are related to kinematical thresholds of the B_0 and C_0 functions of the loop integrals. They are better visualized by the zoomed insets in Fig. 6. In scenario II, the change in $\Delta\Gamma$ when turning from the process-dependent to the ZEM scheme has a large effect. Here, $\Delta\Gamma$ can go from -50% to 10% , whereas in the process-dependent scheme, $\Delta\Gamma$ varies between -3% and 3% . Thus, the ZEM scheme can result in relatively large, with a maximum of 50% , corrections at NLO. These large corrections, however, occur only in a small number of points. These points have a very small tree-level width in the sense that although the ratio of the NLO to the LO width can vary by as much as 50% , the total LO width is nevertheless well below its maximum value of 1 MeV. Also, these are the points that would be rejected by the additional kinematic constraint that in scenario II is effective in the process-dependent scheme. They hence occur only in the ZEM scheme.

One further remark is in order here. One has to be careful when directly comparing the results for $\Delta\Gamma$ in the different renormalization schemes. A consistent comparison would require the proper conversion of the input parameters when going from one scheme to the other. This requires the implementation of the conversion formulas, which is beyond the scope of this paper. Our goal here is to show primarily which sizes of relative corrections at all can be expected in the various schemes. Apart from the ZEM scheme, they are all relatively small and numerically stable in the sense defined above.

In Fig. 7 we present $\Delta\Gamma$ as a function of m_s with all other input parameters fixed. The resulting scenarios do not necessarily fulfill all theoretical or experimental constraints any more but are shown here for illustrative reasons. The

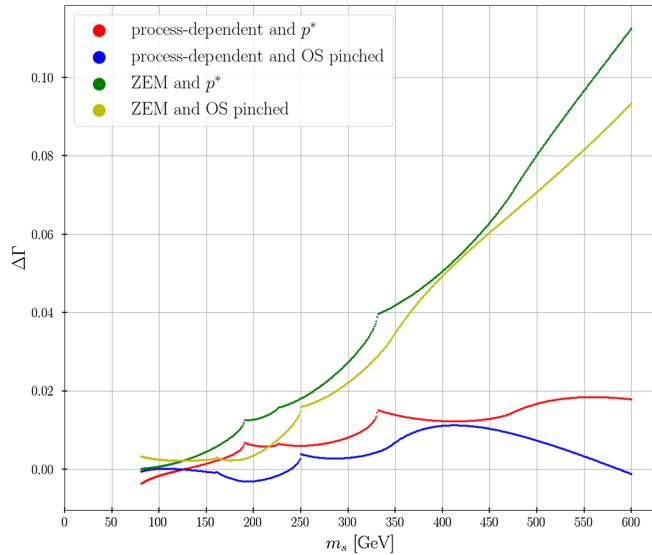


FIG. 7. $\Delta\Gamma$ plotted against the scalar mass m_s , and all other parameters have been set to fixed values, with $\alpha = 0.01$, $v_S = 100$ GeV, and $m_A = 40$ GeV. All possible combinations of renormalization schemes are shown.

peaks that can be seen in the figure originate from thresholds in the loop functions and depend on the chosen scheme as the two schemes used for the derivation of $\delta\alpha$ are evaluated at different scales. For example, the peak in the OS pinched scheme seen in Fig. 7 at $m_S \equiv x_{OS} = 250$ GeV appears in the p^* pinched scheme at the $m_S \equiv x_{p^*}$ value equal to 330 GeV because

$$x_{OS}^2 = \frac{m_{h_{125}}^2 + x_{p^*}^2}{2}, \quad (72)$$

since in the p^* pinched scheme the self-energies are evaluated at the mean of the scalar masses. The peaks only occur in scenario I, because most of the SM masses occurring in the calculation (e.g., the W and Z boson mass) are of order of 100 GeV.

The purpose of this analysis is to improve the precision of the calculation of the Higgs invisible decay width so that it can be used to constrain the parameters from the dark sector. The current observed limit on the branching ratio of the 125 GeV Higgs decay into invisible particles is given by [3]

$$\text{BR}(h_{125} \rightarrow \text{invisible}) \lesssim 0.11_{-0.03}^{+0.04}, \quad (73)$$

at 95% confidence level. To compare results the calculated branching ratio is needed, which in turn means that we need the total decay width of the 125 GeV Higgs boson in the CxSM including NLO EW corrections. Since the corrections are not available for all decays in the model, we can only estimate the branching ratio using the total decay width of the 125 GeV Higgs boson in the SM without EW corrections,¹ which is taken from [53,54] and is given by

$$\Gamma_{h_{125}}^{\text{SM,tot}} = 0.4068 \times 10^{-2} \text{ GeV}. \quad (74)$$

To translate this decay width into the CxSM setup, it will be multiplied by the appropriate squared angular factor k_i^2 , where the index i is chosen according to the mass scenario. Also the NLO $h_{125} \rightarrow AA$ width is added to obtain the total decay width in the CxSM. Furthermore, in scenario II the 125 GeV Higgs boson is the heavier of the two scalar particles ($h_{125} \equiv h_2$). If h_1 is light enough, the decay $h_2 \rightarrow h_1 h_1$ is also allowed and is added to the total decay width. Thus, the LO and approximate NLO branching ratio of the decay $h_{125} \rightarrow AA$ is given by

$$\text{BR}_{\text{CxSM}}^{\text{LO/NLO}}(h_{125} \rightarrow AA) \approx \frac{\Gamma_{h_{125} \rightarrow AA}^{\text{LO/NLO}}}{k_i^2 \Gamma_{h_{125}}^{\text{SM,tot}} + \Gamma_{h_{125} \rightarrow AA}^{\text{LO/NLO}} + \delta\Gamma_{h_{125} \rightarrow h_1 h_1}^{\text{LO}}}, \quad (75)$$

¹It includes, however, the relevant higher-order QCD corrections that can be taken over from the SM to the CxSM.

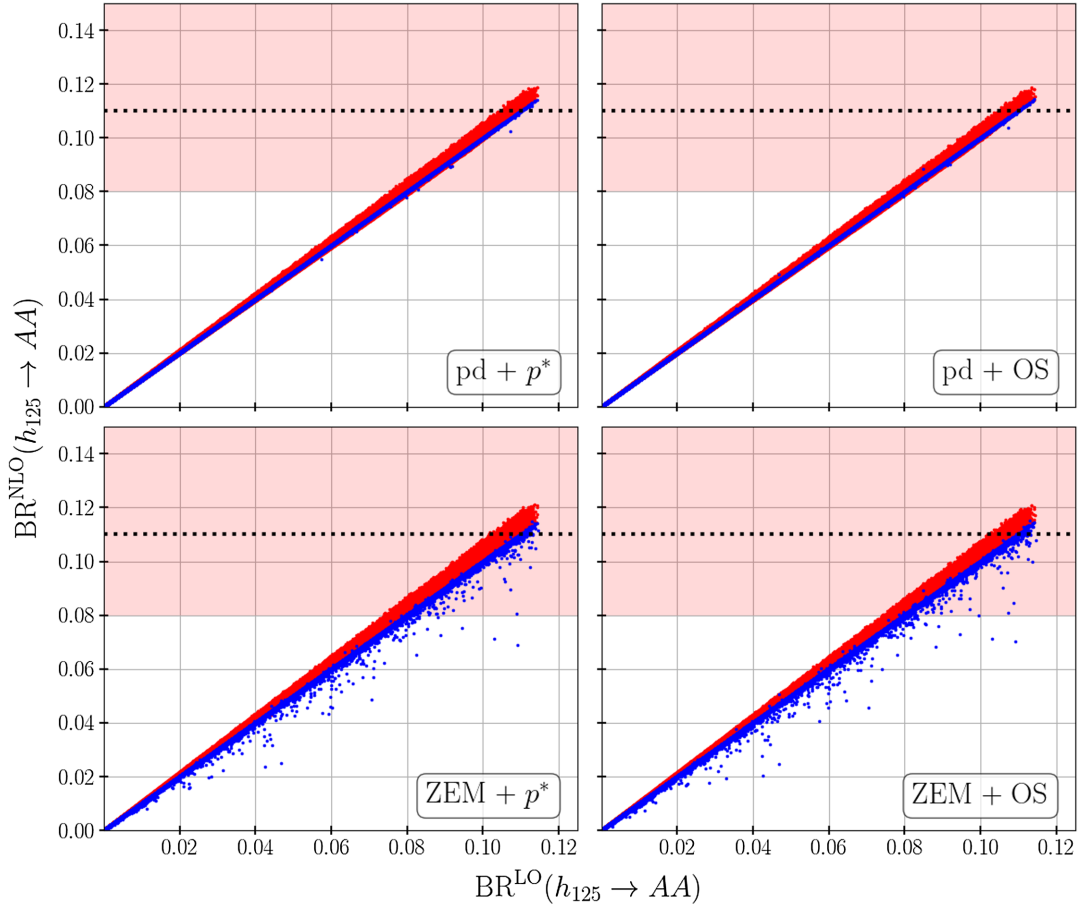


FIG. 8. The calculated branching ratios for the decay $h_{125} \rightarrow AA$ at NLO vs LO for all generated parameter points and all renormalization schemes. The experimental limit is indicated by the dashed line with the uncertainty on the limit given by the red band. Red (blue) points correspond to scenario I (II).

where δ is defined as

$$\delta = \begin{cases} 1, & m_{h_{125}} \geq 2m_s \\ 0, & m_{h_{125}} < 2m_s \end{cases} \quad (76)$$

This expression is approximate in the sense that the NLO EW corrections are only included in the Higgs-to-invisible decay but not in the SM-like CxSM Higgs decays into SM particles. It is justified, however, if the EW corrections to these decay widths are small enough compared to the EW corrections to the $h_{125} \rightarrow AA$ decay.² Moreover, for a better approximation the NLO corrections to the decay $h_{125} \rightarrow h_1 h_1$ have to be included as well unless its contribution to the total width is negligibly small.

In Fig. 8 the calculated approximate NLO branching ratios for all generated parameter points are displayed vs

²From Ref. [55], where for the 2HDM and the N2HDM the EW corrections have been calculated for all the allowed parameter sets and in different renormalization schemes, it can be concluded that the EW corrections to the decay widths of the SM-like Higgs into SM particles amount up to a few percent only.

the corresponding LO values. The experimental limit on the branching ratio is shown as well. However, the limit is only indicated for the NLO result, since the parameter points are generated with respect to the limit at LO. The LO branching ratios hence fulfill all the constraints described in the previous sections and in particular the experimental limit on the Higgs invisible branching ratio. Since the NLO corrections are small, not many points will violate this limit. In fact, almost all parameter points have an NLO branching ratio below the experimental limit. Only about 0.2% of the points are above the experimental limit. The highest obtained branching ratio is, however, around 0.121 and therefore still lies well within the experimental uncertainty. The relative change of the branching ratio at NLO with respect to LO has been calculated and increases the LO value by up to 7%–8% at most. Thus, the NLO contributions to the branching ratio are too small to further constrain the model. Moreover, it is interesting to see that the points from scenario II result in smaller branching ratios, especially when using the ZEM scheme. This is to be expected, since many points in that scenario have negative relative NLO contributions to the decay width.

VI. CONCLUSIONS

In this work we have calculated the EW NLO corrections of the Higgs decay into two dark matter particles in the CxSM. We have used four different renormalization schemes but with all masses and fields renormalized on-shell. Except for very particular regions of the parameter space corresponding to thresholds in the Passarino-Veltman functions, the corrections were shown to be quite small, on the percent level in all renormalization schemes. There is one exception, however, given by the ZEM scheme with h_2 being the SM-like Higgs. Here, points that could not be used in the process-dependent scheme for the renormalization of v_S due to kinematic constraints lead to relatively large corrections that amount up to a few tens of percent.

The central value of the measured invisible Higgs branching ratio is now at 0.11. The inclusion of the EW NLO corrections to the decay width of the process $h_{125} \rightarrow AA$ does not lead to extra constraints on the parameter space because the calculated approximate NLO branching ratios for all allowed parameter points are found to be within the experimental error. Calculating the EW corrections to all decays of the SM-like CxSM Higgs boson into SM particles (and, if kinematically allowed into a pair of lighter scalars) will further improve the obtained result. But more importantly, tighter experimental constraints will be obtained in the near future in the upcoming LHC run [56] and even more at the high luminosity stage.

We have also shown why it is crucial to have a precise measurement of the invisible width—it is the only direct probe of the portal coupling. In fact, the other possible way to probe the same coupling would be through the DM-nucleon cross section. However, we have shown that this cross section is not only below the present experimental bound from XENON1T [11] but is also below the neutrino

floor, which makes it virtually unusable. Therefore, in the near future³ and perhaps also in the far future, information about the dark sector of the CxSM will come only from the LHC. This shows the importance of having the radiative corrections for the invisible Higgs decay.

ACKNOWLEDGMENTS

R. S. and J. V. are supported by FCT under Contracts No. UIDB/00618/2020, No. UIDP/00618/2020, No. PTDC/FIS-PAR/31000/2017, No. CERN/FIS-PAR/0002/2017, and No. CERN/FIS-PAR/0014/2019. The work of F. E. and M. M. is supported by the BMBF-Project No. 05H21VKCCA.

APPENDIX A: THE SCALAR PINCHED SELF-ENERGY IN THE CxSM

In this appendix we will present the result for the scalar pinched self-energy in the CxSM. We define the quantity ($i, j = 1, 2$)

$$O_{ij} \equiv k_i k_j, \quad (\text{A1})$$

to write all couplings in the CxSM between the scalars and the SM particles X, Y as

$$g_{XYh_i} = g_{XYH}^{\text{SM}} k_i, \quad (\text{A2a})$$

$$g_{XYh_i h_j} = g_{XYHH}^{\text{SM}} O_{ij}, \quad (\text{A2b})$$

where g_{XYH}^{SM} and g_{XYHH}^{SM} are the corresponding couplings between the SM particles X and Y and one or two SM Higgs bosons and k_i is given in Eq. (9). With these definitions the self-energies $i\Sigma_{h_i h_j}^{\text{add}}$ are given by

$$\begin{aligned} i\Sigma_{h_i h_j}^{\text{add}}(q^2) &= \frac{-ig^2}{16\pi^2} O_{ij} \left(q^2 - \frac{m_{h_i}^2 + m_{h_j}^2}{2} \right) B_0(q^2, m_W^2, m_W^2) + \frac{-ig^2}{32\pi^2 c_w^2} O_{ij} \left(q^2 - \frac{m_{h_i}^2 + m_{h_j}^2}{2} \right) B_0(q^2, m_Z^2, m_Z^2) \\ &+ \frac{ig^2 \lambda_W}{32\pi^2} O_{ij} \left(\left(q^2 - \frac{m_{h_i}^2 + m_{h_j}^2}{2} \right) \alpha_W - (q^4 - m_{h_i}^2 m_{h_j}^2) \frac{\beta_{WW}(q^2) + \beta_{W\xi_W}(q^2)}{2} \right) \\ &+ \frac{ig^2 \lambda_Z}{64\pi^2 c_w^2} O_{ij} \left(\left(q^2 - \frac{m_{h_i}^2 + m_{h_j}^2}{2} \right) \alpha_Z - (q^4 - m_{h_i}^2 m_{h_j}^2) \frac{\beta_{ZZ}(q^2) + \beta_{Z\xi_Z}(q^2)}{2} \right). \end{aligned}$$

Here $m_{W,Z}$ denote the masses of the W and Z bosons, $g = 2m_W \sqrt{\sqrt{2}G_F}$ is the $SU(2)$ gauge coupling, c_w the cosine of the weak mixing angle, ξ_V ($V = W, Z$) are the bare gauge couplings, and $\lambda_V \equiv 1 - \xi_V$. The integrals are defined as

$$\frac{i}{16\pi^2} B_0(p^2, m_1^2, m_2^2) \equiv \int_k \frac{1}{(k^2 - m_1^2)((k+p)^2 - m_2^2)}, \quad (\text{A3a})$$

$$\frac{i}{16\pi^2} \alpha_V \equiv \int_k \frac{1}{(k^2 - m_V^2)(k^2 - \xi_V m_V^2)}, \quad (\text{A3b})$$

³Recent results from LUX-ZEPLIN [57] do not exclude any of the allowed parameter points since the spin-independent cross sections are still well below the experimental threshold.

$$\begin{aligned} & \frac{i}{16\pi^2} \beta_{V_1 V_2}(p^2) \\ & \equiv \int_k \frac{1}{(k^2 - m_{V_1}^2)(k^2 - \xi_{V_1} m_{V_1}^2)((k+p)^2 - m_{V_2}^2)}, \end{aligned} \quad (\text{A3c})$$

$$\begin{aligned} & \frac{i}{16\pi^2} \beta_{V_1 \xi_{V_2} V_2}(p^2) \\ & \equiv \int_k \frac{1}{(k^2 - m_{V_1}^2)(k^2 - \xi_{V_1} m_{V_1}^2)((k+p)^2 - \xi_{V_2} m_{V_2}^2)}. \end{aligned} \quad (\text{A3d})$$

APPENDIX B: MINIMA OF THE CxSM HIGGS POTENTIAL

To analyze all possible vacuum configurations, the scalar potential of the CxSM,

$$\begin{aligned} V_{\text{scalar}} = & \frac{m^2}{2} \Phi^\dagger \Phi + \frac{\lambda}{4} (\Phi^\dagger \Phi)^2 + \frac{\delta_2}{2} \Phi^\dagger \Phi |\mathbb{S}|^2 + \frac{b_2}{2} |\mathbb{S}|^2 \\ & + \frac{d_2}{4} |\mathbb{S}|^4 + \left(\frac{b_1}{4} \mathbb{S}^2 + \text{c.c.} \right), \end{aligned} \quad (\text{B1})$$

has to be considered with the fields defined as

$$\Phi = \begin{pmatrix} G^+ \\ \frac{1}{\sqrt{2}}(H + iG^0) \end{pmatrix}, \quad \mathbb{S} = \frac{1}{\sqrt{2}}(S + iA). \quad (\text{B2})$$

Because of the $SU(2)$ invariance we can choose a configuration where only the fields H , S , and A can acquire a nonzero VEV, in the following labeled x_H , x_S , and x_A .

The stationary conditions of the potential read

$$\frac{\partial V}{\partial \phi} \Big|_{\langle \phi_i \rangle = x_i} = 0 \Rightarrow \begin{cases} \frac{m^2}{2} x_H + \frac{\lambda}{4} x_H^3 + \frac{\delta_2}{4} x_H (x_S^2 + x_A^2) = 0 \\ \frac{b_1 + b_2}{2} x_S + \frac{d_2}{4} x_S (x_S^2 + x_A^2) + \frac{\delta_2}{4} x_S x_H^2 = 0 \\ \frac{b_2 - b_1}{2} x_A + \frac{d_2}{4} x_A (x_S^2 + x_A^2) + \frac{\delta_2}{4} x_A x_H^2 = 0 \\ 0 = 0 \\ 0 = 0 \\ 0 = 0 \end{cases}, \quad (\text{B3})$$

with the scalar fields collected in the vector $[G^+ \equiv 1/\sqrt{2}(G_1 - iG_2)]$

$$\vec{\phi} = (H, S, A, G^0, G_1, G_2)^T. \quad (\text{B4})$$

The three nontrivial equations in Eq. (B3) can be written as

$$x_H \left(\frac{m^2}{2} + \frac{\lambda}{4} x_H^2 + \frac{\delta_2}{4} (x_S^2 + x_A^2) \right) = 0, \quad (\text{B5a})$$

$$x_S \left(\frac{b_1 + b_2}{2} + \frac{d_2}{4} (x_S^2 + x_A^2) + \frac{\delta_2}{4} x_H^2 \right) = 0, \quad (\text{B5b})$$

$$x_A \left(\frac{b_2 - b_1}{2} + \frac{d_2}{4} (x_S^2 + x_A^2) + \frac{\delta_2}{4} x_H^2 \right) = 0, \quad (\text{B5c})$$

from which we read off that for all VEVs a possible solution is to set them to zero or solve the equations in brackets. Thus, eight different cases, in general, have to be considered. Moreover, if x_S and x_A are simultaneously nonzero, the terms in brackets in Eqs. (B5b) and (B5c) have to be zero. Since these two terms differ only in the sign in front of the parameter b_1 , this can be achieved only if b_1 is set to zero. Here, however, b_1 is always chosen to be nonzero, and thus these cases cannot result in a minimum of the potential.

Furthermore, it has to be checked whether the stationary point is indeed a minimum of the potential, i.e., the Hessian matrix of the potential has to be positive definite. The general form of the Hessian matrix reads

$$V_{\text{Hesse}} = \begin{pmatrix} A & \frac{\delta_2 x_H x_S}{2} & \frac{\delta_2 x_H x_A}{2} & 0 & 0 & 0 \\ \frac{\delta_2 x_H x_S}{2} & B & \frac{d_2 x_S x_A}{2} & 0 & 0 & 0 \\ \frac{\delta_2 x_H x_A}{2} & \frac{d_2 x_S x_A}{2} & C & 0 & 0 & 0 \\ 0 & 0 & 0 & D & 0 & 0 \\ 0 & 0 & 0 & 0 & D & 0 \\ 0 & 0 & 0 & 0 & 0 & D \end{pmatrix}, \quad (\text{B6})$$

where the diagonal elements are

$$A = \frac{m^2}{2} + \frac{\delta_2 (x_S^2 + x_A^2)}{4} + \frac{3\lambda x_H^2}{4}, \quad (\text{B7a})$$

$$B = \frac{b_1 + b_2}{2} + \frac{d_2 (3x_S^2 + x_A^2)}{4} + \frac{\delta_2 x_H^2}{4}, \quad (\text{B7b})$$

$$C = \frac{-b_1 + b_2}{2} + \frac{d_2 (x_S^2 + 3x_A^2)}{4} + \frac{\delta_2 x_H^2}{4}, \quad (\text{B7c})$$

$$D = \frac{m^2}{2} + \frac{\delta_2 (x_A^2 + x_S^2)}{4} + \frac{\lambda x_H^2}{4}. \quad (\text{B7d})$$

To start with the remaining cases, first the desired minimum is considered, namely the configuration with the VEVs x_H and x_S to be nonzero and x_A to be zero. Since the VEVs are chosen to be input parameters, they are in this case relabeled as v and v_S and the Eqs. (B5) can be solved for other parameters resulting in

$$m^2 = \frac{-1}{2}(\lambda v^2 + \delta_2 v_S^2), \quad b_1 + b_2 = \frac{-1}{2}(d_2 v_S^2 + \delta_2 v^2). \quad (\text{B8})$$

Next, the positive definiteness of the Hessian matrix has to be checked. For this Eq. (B8) is used to simplify the Hessian matrix in Eq. (B6) leading to

$$V_{\text{Hesse}}(x_H = v, x_S = v_S, x_A = 0) = \begin{pmatrix} \frac{\lambda v^2}{2} & \frac{\delta_2 v v_S}{2} & 0 & 0 & 0 & 0 \\ \frac{\delta_2 v v_S}{2} & \frac{d_2 v_S^2}{2} & 0 & 0 & 0 & 0 \\ 0 & 0 & -b_1 & 0 & 0 & 0 \\ 0 & 0 & 0 & 0 & 0 & 0 \\ 0 & 0 & 0 & 0 & 0 & 0 \\ 0 & 0 & 0 & 0 & 0 & 0 \end{pmatrix}. \quad (\text{B9})$$

The matrix is positive definite if the determinants of all minors are positive; i.e., the relations

$$\lambda > 0 \wedge d_2 > 0 \wedge \lambda d_2 > \delta_2^2 \wedge b_1 < 0 \quad (\text{B10})$$

have to be satisfied. If these inequalities hold, the potential is automatically bounded from below [compare with Eq. (52)]. Moreover, the Hessian matrix of the potential resembles the mass matrix of the scalar fields; i.e., the eigenvalues of the matrix are the squared masses of the corresponding particles, and thus the eigenvalues have to be positive; i.e., the Hessian matrix has to be positive definite. Furthermore, the parameter b_1 is just given by $-m_A^2$.

This means that if the VEVs v and v_S are given as input parameters, the VEV for the field A is chosen to be zero, and the potential parameters fulfill the relations in Eq. (B10), this configuration of VEVs is a minimum of the potential, as desired. The remaining question now is, whether this minimum is automatically the global minimum of the potential. Thus, the values of the potential at all minimum configurations have to be calculated and compared. For the desired configuration the value of the potential at the minimum reads

$$\begin{aligned} V(x_H = v, x_S = v_S, x_A = 0) &= V(v, v_S, 0) \\ &= -\frac{1}{16}(\lambda v^4 + 2\delta_2 v^2 v_S^2 + d_2 v_S^4). \end{aligned} \quad (\text{B11})$$

Now all other VEV configurations have to be checked for their potential values at the stationary point and whether they are indeed a minimum of the potential.

(i) Case $x_H = x_S = x_A = 0$:

This is the most trivial configuration, and the value of the potential at this point reads

$$V(0, 0, 0) = 0. \quad (\text{B12})$$

Thus, the difference between the values of the potential at the two configurations results in

$$\begin{aligned} V(v, v_S, 0) - V(0, 0, 0) \\ &= -\frac{1}{16}(\lambda v^4 + 2\delta_2 v^2 v_S^2 + d_2 v_S^4) < 0. \end{aligned} \quad (\text{B13})$$

The inequality is true because of the relation among δ_2 , λ , and d_2 from Eq. (B10).

(ii) Case $x_S = x_A = 0, x_H \neq 0$:

Here the nontrivial equation from Eqs. (B5) can be solved for x_H and results in

$$x_H = \sqrt{\frac{-2m^2}{\lambda}} \equiv x_1. \quad (\text{B14})$$

Here m^2 has to be negative. The value of the potential results in

$$V(x_1, 0, 0) = \frac{-m^4}{4\lambda} = -\frac{(\lambda v^2 + \delta_2 v_S^2)^2}{16\lambda}, \quad (\text{B15})$$

where in the second step the relations Eq. (B8) were used. The difference between the values of the potential of the different configurations reads

$$V(v, v_S, 0) - V(x_1, 0, 0) = -\frac{(d_2 \lambda - \delta_2^2) v_S^4}{16\lambda} < 0. \quad (\text{B16})$$

The inequality again holds because of the relations Eq. (B10).

(iii) Case $x_H = x_A = 0, x_S \neq 0$:

Here the nontrivial equation from Eqs. (B5) can be solved for x_S and results in

$$x_S = \sqrt{\frac{-2(b_1 + b_2)}{d_2}} \equiv x_2. \quad (\text{B17})$$

Here $b_1 + b_2$ has to be negative. The value of the potential results in

$$V(0, x_2, 0) = -\frac{(b_1 + b_2)^2}{4d_2} = -\frac{(\delta_2 v^2 + d_2 v_S^2)^2}{16d_2}, \quad (\text{B18})$$

where in the second step the relations Eq. (B8) were used. The difference between the values of the potential of the different configurations reads

$$V(v, v_S, 0) - V(0, x_2, 0) = -\frac{(d_2\lambda - \delta_2^2)v^4}{16d_2} < 0. \quad (\text{B19})$$

The inequality again holds because of the relations Eq. (B10).

(iv) Case $x_H = x_S = 0, x_A \neq 0$:

Here the nontrivial equation from Eqs. (B5) can be solved for x_A and results in

$$x_A = \sqrt{\frac{-2(b_2 - b_1)}{d_2}} \equiv x_3. \quad (\text{B20})$$

Here $b_2 - b_1$ has to be negative. The value of the potential results in

$$\begin{aligned} V(0, 0, x_3) &= -\frac{(b_2 - b_1)^2}{4d_2} \\ &= -\frac{(4b_1 + \delta_2 v^2 + d_2 v_S^2)^2}{16d_2}, \end{aligned} \quad (\text{B21})$$

where in the second step the relations Eq. (B8) were used. Here the parameter b_1 does not get canceled and the difference between the values of the potential of this configuration with respect to the desired minimum state depends additionally on b_1 and an inequality similar to the other cases cannot be shown as straightforwardly. It is, however, sufficient to look at the Hessian matrix. It results in

$$V_{\text{Hesse}}(0, 0, x_3) = \begin{pmatrix} E & 0 & 0 & 0 & 0 & 0 \\ 0 & b_1 & 0 & 0 & 0 & 0 \\ 0 & 0 & b_1 - b_2 & 0 & 0 & 0 \\ 0 & 0 & 0 & E & 0 & 0 \\ 0 & 0 & 0 & 0 & E & 0 \\ 0 & 0 & 0 & 0 & 0 & E \end{pmatrix}, \quad (\text{B22})$$

where E is a combination of potential parameters. It can be seen that b_1 is a negative eigenvalue of the matrix. Thus, it cannot be positive definite, and this VEV configuration cannot be a minimum.

(v) Case $x_S = 0, x_H \neq 0, x_A \neq 0$:

The last case is a bit more complicated, since now two VEVs are nonzero. Here it is easier to redo the

same steps as in the desired minimum configuration. First, the VEVs are relabeled as w and w_A . Next, the stationary conditions from Eqs. (B5) are solved for other parameters to obtain the relations

$$\begin{aligned} m^2 &= -\frac{1}{2}(\lambda w^2 + \delta_2 w_A^2), \\ b_2 - b_1 &= -\frac{1}{2}(\delta_2 w^2 + d_2 w_A^2). \end{aligned} \quad (\text{B23})$$

Similar to the last case, the value of the potential of this configuration will again depend on b_1 , so comparing values with the desired minimum configuration will not lead to a simple inequality. Thus, the Hessian matrix is again considered. With the help of Eqs. (B23) it can be simplified to

$$V_{\text{Hesse}}(w, 0, w_A) = \begin{pmatrix} \frac{\lambda w^2}{2} & 0 & \frac{\delta_2 w w_A}{2} & 0 & 0 & 0 \\ 0 & b_1 & 0 & 0 & 0 & 0 \\ \frac{\delta_2 w w_A}{2} & 0 & \frac{d_2 w_A^2}{2} & 0 & 0 & 0 \\ 0 & 0 & 0 & 0 & 0 & 0 \\ 0 & 0 & 0 & 0 & 0 & 0 \\ 0 & 0 & 0 & 0 & 0 & 0 \end{pmatrix}. \quad (\text{B24})$$

Again, b_1 is a negative eigenvalue of the matrix; thus, it cannot be a positive definite matrix and the configuration is not a minimum.

Moreover, the similarity between the two cases with two nonzero VEVs is interesting. If the configuration with w and w_A would be chosen as the desired minimum configuration, then b_1 would necessarily be positive and the minimum configuration with v and v_S would no longer be a minimum. The sign in front of b_1 is essentially the only difference between the fields S and A and therefore also the only difference between these VEV configurations.

To conclude, if the nonzero VEV parameters v and v_S are given as input parameters and the remaining potential parameters are chosen such that the relations Eq. (B10) are fulfilled, then this configuration is a minimum of the potential, and it is the global minimum (the potential is also bounded from below with the same relations, so it really is the global minimum of the potential).

- [1] G. Aad *et al.* (ATLAS Collaboration), Observation of a new particle in the search for the Standard Model Higgs boson with the ATLAS detector at the LHC, *Phys. Lett. B* **716**, 1 (2012).
- [2] S. Chatrchyan *et al.* (CMS Collaboration), Observation of a new boson at a mass of 125 GeV with the CMS experiment at the LHC, *Phys. Lett. B* **716**, 30 (2012).
- [3] M. Aaboud *et al.* (ATLAS Collaboration), Combination of Searches for Invisible Higgs Boson Decays with the ATLAS Experiment, *Phys. Rev. Lett.* **122**, 231801 (2019).
- [4] G. Arcadi, A. Djouadi, and M. Raidal, Dark matter through the Higgs portal, *Phys. Rep.* **842**, 1 (2020).
- [5] O. Lebedev, The Higgs portal to cosmology, *Prog. Part. Nucl. Phys.* **120**, 103881 (2021).
- [6] D. Azevedo, P. Gabriel, M. Muhlleitner, K. Sakurai, and R. Santos, One-loop corrections to the Higgs boson invisible decay in the dark doublet phase of the N2HDM, *J. High Energy Phys.* **10** (2021) 044.
- [7] C. Gross, O. Lebedev, and T. Toma, Cancellation Mechanism for Dark-Matter–Nucleon Interaction, *Phys. Rev. Lett.* **119**, 191801 (2017).
- [8] D. Azevedo, M. Duch, B. Grzadkowski, D. Huang, M. Iglicki, and R. Santos, Testing scalar versus vector dark matter, *Phys. Rev. D* **99**, 015017 (2019).
- [9] D. Azevedo, M. Duch, B. Grzadkowski, D. Huang, M. Iglicki, and R. Santos, One-loop contribution to dark-matter-nucleon scattering in the pseudo-scalar dark matter model, *J. High Energy Phys.* **01** (2019) 138.
- [10] S. Glaus, M. Muhlleitner, J. Müller, S. Patel, T. Römer, and R. Santos, Electroweak corrections in a pseudo-Nambu Goldstone dark matter model revisited, *J. High Energy Phys.* **12** (2020) 034.
- [11] E. Aprile *et al.* (XENON Collaboration), Dark Matter Search Results from a One Ton-Year Exposure of XENON1T, *Phys. Rev. Lett.* **121**, 111302 (2018).
- [12] P. Athron *et al.* (GAMBIT Collaboration), Status of the scalar singlet dark matter model, *Eur. Phys. J. C* **77**, 568 (2017).
- [13] L. Coito, C. Faubel, J. Herrero-Garcia, and A. Santamaria, Dark matter from a complex scalar singlet: The role of dark CP and other discrete symmetries, *J. High Energy Phys.* **11** (2021) 202.
- [14] R. Costa, M. Muhlleitner, M. O. P. Sampaio, and R. Santos, Singlet extensions of the Standard Model at LHC Run 2: Benchmarks and comparison with the NMSSM, *J. High Energy Phys.* **06** (2016) 034.
- [15] J. Fleischer and F. Jegerlehner, Radiative corrections to Higgs decays in the extended Weinberg-Salam model, *Phys. Rev. D* **23**, 2001 (1981).
- [16] D. S. de Sousa Machado Fontes, Multi-Higgs models: Model building, phenomenology and renormalization. Ph.D. thesis, University of Lisbon (main) [arXiv:2109.08394].
- [17] M. Krause, R. Lorenz, M. Muhlleitner, R. Santos, and H. Ziesche, Gauge-independent renormalization of the 2-Higgs-doublet model, *J. High Energy Phys.* **09** (2016) 143.
- [18] M. Krause, D. Lopez-Val, M. Muhlleitner, and R. Santos, Gauge-independent renormalization of the N2HDM, *J. High Energy Phys.* **12** (2017) 077.
- [19] S. Kanemura, Y. Okada, E. Senaha, and C. P. Yuan, Higgs coupling constants as a probe of new physics, *Phys. Rev. D* **70**, 115002 (2004).
- [20] A. Pilaftsis, Resonant CP violation induced by particle mixing in transition amplitudes, *Nucl. Phys.* **B504**, 61 (1997).
- [21] J. M. Cornwall and J. Papavassiliou, Gauge invariant three gluon vertex in QCD, *Phys. Rev. D* **40**, 3474 (1989).
- [22] J. Papavassiliou, Gauge independent transverse and longitudinal self-energies and vertices via the pinch technique, *Phys. Rev. D* **50**, 5958 (1994).
- [23] J. Papavassiliou, Gauge invariant proper self-energies and vertices in gauge theories with broken symmetry, *Phys. Rev. D* **41**, 3179 (1990).
- [24] D. Binosi and J. Papavassiliou, Pinch technique: Theory and applications, *Phys. Rep.* **479**, 1 (2009).
- [25] R. Coimbra, M. O. P. Sampaio, and R. Santos, ScannerS: Constraining the phase diagram of a complex scalar singlet at the LHC, *Eur. Phys. J. C* **73**, 2428 (2013).
- [26] R. Costa, A. P. Morais, M. O. P. Sampaio, and R. Santos, Two-loop stability of a complex singlet extended standard model, *Phys. Rev. D* **92**, 025024 (2015).
- [27] M. Muhlleitner, M. O. P. Sampaio, R. Santos, and J. Wittbrodt, ScannerS: Parameter scans in extended scalar sectors, *Eur. Phys. J. C* **82**, 198 (2022).
- [28] B. W. Lee, C. Quigg, and H. B. Thacker, Weak interactions at very high-energies: The role of the Higgs boson mass, *Phys. Rev. D* **16**, 1519 (1977).
- [29] M. E. Peskin and T. Takeuchi, Estimation of oblique electroweak corrections, *Phys. Rev. D* **46**, 381 (1992).
- [30] P. Bechtle, S. Heinemeyer, O. Stål, T. Stefaniak, and G. Weiglein, HiggsSignals: Confronting arbitrary Higgs sectors with measurements at the Tevatron and the LHC, *Eur. Phys. J. C* **74**, 2711 (2014).
- [31] P. Bechtle, S. Heinemeyer, T. Klingl, T. Stefaniak, G. Weiglein, and J. Wittbrodt, HiggsSignals-2: Probing new physics with precision Higgs measurements in the LHC 13 TeV era, *Eur. Phys. J. C* **81**, 145 (2021).
- [32] P. Bechtle, O. Brein, S. Heinemeyer, G. Weiglein, and K. E. Williams, HiggsBounds: Confronting arbitrary Higgs sectors with exclusion bounds from LEP and the Tevatron, *Comput. Phys. Commun.* **181**, 138 (2010).
- [33] P. Bechtle, D. Dercks, S. Heinemeyer, T. Klingl, T. Stefaniak, G. Weiglein, and J. Wittbrodt, HiggsBounds-5: Testing Higgs sectors in the LHC 13 TeV era, *Eur. Phys. J. C* **80**, 1211 (2020).
- [34] G. Belanger, F. Boudjema, A. Pukhov, and A. Semenov, MicrOMEGAs 2.0: A program to calculate the relic density of dark matter in a generic model, *Comput. Phys. Commun.* **176**, 367 (2007).
- [35] N. D. Christensen and C. Duhr, FeynRules—Feynman rules made easy, *Comput. Phys. Commun.* **180**, 1614 (2009).
- [36] C. Degrande, C. Duhr, B. Fuks, D. Grellscheid, O. Mattelaer, and T. Reiter, UFO—the Universal FeynRules Output, *Comput. Phys. Commun.* **183**, 1201 (2012).
- [37] A. Alloul, N. D. Christensen, C. Degrande, C. Duhr, and B. Fuks, FeynRules 2.0—a complete toolbox for tree-level phenomenology, *Comput. Phys. Commun.* **185**, 2250 (2014).
- [38] J. Kublbeck, M. Bohm, and A. Denner, FeynArts: Computer algebraic generation of Feynman graphs and amplitudes, *Comput. Phys. Commun.* **60**, 165 (1990).
- [39] T. Hahn, Generating Feynman diagrams and amplitudes with FeynArts 3, *Comput. Phys. Commun.* **140**, 418 (2001).

- [40] R. Mertig, M. Bohm, and A. Denner, FeynCalc: Computer algebraic calculation of Feynman amplitudes, *Comput. Phys. Commun.* **64**, 345 (1991).
- [41] V. Shtabovenko, R. Mertig, and F. Orellana, New developments in FeynCalc 9.0, *Comput. Phys. Commun.* **207**, 432 (2016).
- [42] T. Hahn and M. Perez-Victoria, Automatized one loop calculations in four-dimensions and D-dimensions, *Comput. Phys. Commun.* **118**, 153 (1999).
- [43] G. J. van Oldenborgh and J. A. M. Vermaseren, New algorithms for one loop integrals, *Z. Phys. C* **46**, 425 (1990).
- [44] F. Staub, From superpotential to model files for FeynArts and CalcHep/CompHep, *Comput. Phys. Commun.* **181**, 1077 (2010).
- [45] F. Staub, Automatic calculation of supersymmetric renormalization group equations and self-energies, *Comput. Phys. Commun.* **182**, 808 (2011).
- [46] F. Staub, SARAH 3.2: Dirac gauginos, UFO output, and more, *Comput. Phys. Commun.* **184**, 1792 (2013).
- [47] F. Staub, SARAH 4: A tool for (not only SUSY) model builders, *Comput. Phys. Commun.* **185**, 1773 (2014).
- [48] F. Staub, Exploring new models in all detail with SARAH, *Adv. High Energy Phys.* **2015**, 840780 (2015).
- [49] P. Zyla *et al.* (Particle Data Group), Review of particle physics, *Prog. Theor. Exp. Phys.* **2020**, 083C01 (2020).
- [50] P. Basler and M. Mühlleitner, BSMPT (Beyond the Standard Model Phase Transitions): A tool for the electroweak phase transition in extended Higgs sectors, *Comput. Phys. Commun.* **237**, 62 (2019).
- [51] P. Basler, M. Mühlleitner, and J. Müller, BSMPT v2 a tool for the electroweak phase transition and the baryon asymmetry of the universe in extended Higgs Sectors, *Comput. Phys. Commun.* **269**, 108124 (2021).
- [52] J. Billard, L. Strigari, and E. Figueroa-Feliciano, Implication of neutrino backgrounds on the reach of next generation dark matter direct detection experiments, *Phys. Rev. D* **89**, 023524 (2014).
- [53] A. Djouadi, J. Kalinowski, and M. Spira, HDECAY: A program for Higgs boson decays in the Standard Model and its supersymmetric extension, *Comput. Phys. Commun.* **108**, 56 (1998).
- [54] A. Djouadi, J. Kalinowski, M. Mühlleitner, and M. Spira, HDECAY: Twenty + + years after, *Comput. Phys. Commun.* **238**, 214 (2019).
- [55] M. Krause and M. Mühlleitner, Impact of electroweak corrections on neutral Higgs boson decays in extended Higgs sectors, *J. High Energy Phys.* **04** (2020) 083.
- [56] D. de Florian *et al.* (LHC Higgs Cross Section Working Group), Handbook of LHC Higgs Cross Sections: 4. Deciphering the Nature of the Higgs Sector, Report No. CERN-2017-002-M, CERN-2017-002, CERN, 2016, 10.23731/CYRM-2017-002.
- [57] J. Aalbers *et al.*, First dark matter search results from the Lux-Zeplin (lz) experiment, [arXiv:2207.03764](https://arxiv.org/abs/2207.03764).